

Cosmic ray production in supernovae

A.M. Bykov · D.C. Ellison · A. Marcowith ·
S.M. Osipov

Received: 4 December 2017 / Accepted in Space Science Reviews: 24 January 2018

Supernovae
Edited by Andrei Bykov, Roger Chevalier, John Raymond, Friedrich-Karl Thielemann, Maurizio Falanga
and Rudolf von Steiger

Abstract We give a brief review of the origin and acceleration of cosmic rays (CRs), emphasizing the production of CRs at different stages of supernova evolution by the first-order Fermi shock acceleration mechanism. We suggest that supernovae with trans-relativistic outflows, despite being rather rare, may accelerate CRs to energies above 10^{18} eV over the first year of their evolution. Supernovae in young compact clusters of massive stars, and interaction powered superluminous supernovae, may accelerate CRs well above the PeV regime. We discuss the acceleration of the bulk of the galactic CRs in isolated supernova remnants and re-acceleration of escaped CRs by the multiple shocks present in superbubbles produced by associations of OB stars. The effects of magnetic field amplification by CR driven instabilities, as well as superdiffusive CR transport, are discussed for nonthermal radiation produced by nonlinear shocks of all speeds including trans-relativistic ones.

Keywords Supernovae · Cosmic Rays · Supernova remnants · Interstellar medium · magnetic turbulence

1 Introduction

Based on early inconclusive evidence, Baade & Zwicky (1934) suggested that cosmic rays (CRs) are produced by supernovae (SNe). Since then it has become clear that SNe are the most likely source of CRs, at least for those with energies below the so-called “knee” at $\sim 10^{15}$ eV, for four main reasons. First, and most important, SNe are the only known galactic source with sufficient energy to power CRs (e.g., Ginzburg & Syrovatskii 1964, Axford 1981, Berezhinskii et al. 1990, Hillas 2005, Reynolds 2008, Lingenfelter 2017). Even for supernova remnants (SNRs) the acceleration of CRs must be highly efficient. Second, the source composition of the bulk of CR material is primarily well-mixed interstellar medium (ISM)

A.M. Bykov
Ioffe Institute, 194021, St. Petersburg, Russia; ambykov@yahoo.com;

D.C. Ellison
North Carolina State University, Department of Physics, Raleigh, NC 27695-8202, USA;
don_ellison@ncsu.edu

A. Marcowith
Laboratoire Univers et Particules de Montpellier CNRS/Universite de Montpellier, Place E. Bataillon,
34095 Montpellier, France; Alexandre.Marcowith@umontpellier.fr

S.M. Osipov
Ioffe Institute, 194021, St. Petersburg, Russia; osm2004@mail.ru

material (including those elements preferentially locked in dust) with no more than a 20% contribution from fresh core-collapse SN ejecta material (i.e., Meyer et al. 1997, Ellison et al. 1997, Meyer & Ellison 1999, Binns et al. 2014). This requires a source that injects *old* (i.e., not freshly synthesized) material from the entire galaxy including material from low-mass stars that never explode. No source other than SNRs has a galactic filling factor large enough to do this. Third, there is now a wealth of observational evidence from SNRs showing non-thermal radiation emitted by ultra-relativistic electrons and ions (e.g., Helder et al. 2012, Ackermann et al. 2013b, Blasi 2013, Amato 2014, Blandford et al. 2014, Slane et al. 2015b). The *in situ* production of CRs is observed in SNRs! Fourth, the collisionless shocks associated with SNRs can utilize the first-order Fermi shock acceleration mechanism to simultaneously accelerate various ion species with high efficiency (e.g., Ahn et al. 2010). Perhaps even more important, for the same set of parameters, first-order Fermi shock acceleration accelerates electrons and ions with similar spectral shapes, as observed in CRs and solar energetic particles (e.g., Ellison & Ramaty 1985, Boyle et al. 2008). No other mechanism as naturally produces similar spectral shapes for leptons and hadrons.

The power required to maintain the observed energy density of CRs (dominated by nuclei in the GeV range) is $\sim 2 \times 10^{41} \text{ erg s}^{-1}$ (e.g., Berezhinskii et al. 1990). This is estimated by assuming some CR propagation model with the CR escape length from the galaxy derived from the observed secondary to primary nuclei ratio (e.g., Ptuskin 2012, Aharonian et al. 2012). If in the Milky Way, there is one SN every 30–100 yr with an average kinetic energy of 2×10^{51} erg, an efficiency of 10–30% is required to power CRs, i.e., $> 10\%$ of the ram kinetic energy of the SNR blast wave must be put into relativistic particles of the GeV energy regime.

If acceleration efficiencies are this large, nonlinear feedback effects from CR production will influence the shock dynamics and the resultant CR spectral shape (e.g., Berezhko & Ellison 1999). Consequences for the dynamics include the fact that the test-particle relation between the postshock temperature, T_2 , and the shock speed, u_0 , often assumed for strong shocks, will be modified, i.e., $(1/\mu m_H)(kT_2/u_0^2 \neq 3/16)$ (e.g., Decourchelle et al. 2000, Hughes et al. 2000). Here μm_H is the mean particle mass. Likewise, the Sedov solutions relating the SNR age to the shock radius and speed will also be modified (e.g., Ellison et al. 2007).

Recent detailed observations of the energy spectrum, composition, and anisotropy of the angular distribution of CRs up to TeV energies have been made by spacecraft and balloon instruments, e.g., *ACE*, *PAMELA*, *AMS2*, *CREAM*, *SuperTIGER*, and *Fermi*. For higher energies, ground-based experiments are required and these include *KASCADE-Grande*, *TUNKA*, and *LOFAR* up to a few hundred PeV, while the *Telescope Array* and the *Pierre Auger* observatories provided detailed CR observations to EeV energies. The *LOFAR* array measures radio emission produced by relativistic leptons created in high-energy CR air showers. This relatively new technique has a large duty cycle and can determine the atmospheric depth of shower maximum, and thus CR energy, with high resolution (Buitink et al. 2016). The high statistics of the above mentioned measurements have allowed a closer look into the spectral features which have long been used to understand the sources of CRs, their propagation in the Galaxy and beyond, and the assumed transition from a galactic source to extragalactic sources of CRs above $\sim 10^{18}$ eV (e.g., Bergman & Belz 2007, Lipari 2017).

A particularly interesting feature has been the spectral hardening of protons and helium at rigidities above ~ 230 GV reported by *PAMELA* and *AMS2*.¹ This hardening is likely fairly broad and may extend beyond the rigidity range of both *PAMELA* and *AMS2*. The combined fit of *AMS2* and *CREAM* data made by Lipari (2017) indicates a very broad feature that extends from 200 GeV to 2 TeV with a spectral index difference of ~ 0.2 (see Malkov 2017).

Other important features in the all particle spectrum are the so-called “knee” at 10^{15-16} eV and the “ankle” in the EeV range. The energy band between the knee and the ankle is crucial for understanding the transition between galactic and extragalactic CRs (e.g., Bergman & Belz 2007, Aloisio et al. 2007). Regardless of the energy range, and despite decades of portraying the all particle spectrum observed at Earth as a simple power law, improved statistics are

¹ Rigidity is defined as pc/Ze where p is the particle momentum, c is the speed of light, e is the electronic charge, Z is the total charge number of the particle, and the units are volts.

beginning to show that irregularities and substructures are present in the spectrum (e.g., Apel et al. 2013, Berezhnev et al. 2012).

Recent high resolution measurements by the *LOFAR* telescope below ~ 1 EeV (Buitink et al. 2016) favor a CR composition with a light-mass fraction (protons and helium nuclei) of about 80%. A light-mass fraction this high is surprising and may show the existence of an extra-galactic component at energies between the knee and the ankle, or a previously unsuspected light-mass galactic CR component at these energies (e.g., Thoudam et al. 2016).

Another important measurement is the anisotropy. This is below a few percent for CR energies $\lesssim 1$ EeV. The data thus far does not allow clear conclusions at higher energies but recent observations have shown a large-scale anisotropy with an amplitude of $\sim 10^{-3}$, along with small-scale structure (angular size $10^\circ - 30^\circ$) at about the 10^{-4} level (i.e., Abeysekara et al. 2017). It is still not possible to constrain particular source populations, or specific nearby sources, from the anisotropy observations.

The direct observation of CRs can only be done at the Earth since the charged CRs meander through the irregular galactic magnetic field and virtually all directional information from the source is lost. Source information can be obtained, however, by observing the non-thermal radiation CRs produce in specific objects such as SNRs. Multi-wavelength observations of SNRs give detailed information on the CR acceleration process. Diffuse galactic emission on the other hand gives direct information on the distribution of CRs throughout the galaxy.

Recent observations of non-thermal radiation from young (< 1000 yr) and middle-aged SNRs have proven that particles are accelerated to above 10 TeV by the shocks in these objects. Synchrotron radiation from relativistic leptons is detected from radio to X-rays, and the high angular resolution observations by *VLA* and *Chandra* of young SNRs like Tycho's SNR, Cas A, SN1006, and RX J1713.7-3946 provide compelling evidence for magnetic field amplification (MFA) directly associated with the acceleration process at the remnant forward shock (e.g., Reynolds 2008, Vink 2012, Helder et al. 2012).

The Fermi acceleration process (i.e., Fermi 1949, 1954), and its particular realization called diffusive shock acceleration (DSA) (Axford et al. 1977, Krymskii 1977, Bell 1978, Blandford & Ostriker 1978), provides a plausible way to efficiently convert the kinetic energy released in a supernova shock to a wide energy spectrum of accelerated particles (e.g., Blandford & Eichler 1987, Jones & Ellison 1991, Malkov & Drury 2001, Schure et al. 2012). In fact, Fermi acceleration can occur at any collisionless shock and there is direct observational confirmation of efficient particle acceleration at the quasi-parallel Earth bow shock (i.e., Ellison et al. 1990).²

The forward shocks in most galactic SNRs are observed to have speeds below $\sim 10^4$ km s^{-1} . While these shocks are believed to be capable of producing the bulk of galactic CRs to energies approaching the knee via Fermi acceleration uncertainties remain. It is still uncertain how particles escape from the accelerator without experiencing strong adiabatic losses, and the maximum CR energy produced in observed SNRs does not extend into the knee. Particle escape depends on the galactic environment at the late stages of SNR evolution which may be in the warm ISM or in a superbubble produced by clustered SNe (e.g., Mac Low & McCray 1988, Heiles 1990, Cox 2005). As for the maximum CR energy a given shock can produce, E_{\max} , Lagage & Cesarsky (1983) estimated E_{\max} for Fermi acceleration at the forward shock of an isolated SNR over its lifetime as $E_{\max} \sim 10^5 Z B_{-6}$ GeV, where Z is the ion charge number and B_{-6} is the ISM magnetic field measured in μ G (see also Hillas 2005).

The γ -ray observations of SNRs W44 and IC 443 provide clear evidence for pion production in a SNR due to TeV CR proton interactions (Giuliani et al. 2011, Ackermann et al. 2013b). The evidence for PeV CRs is less certain. All of the SNRs identified so far show breaks in their

² We note that while the terms ‘‘Fermi acceleration’’ and ‘‘diffusive shock acceleration’’ are often used interchangeably there is an important difference when relativistic shocks are discussed. Particle transport in relativistic flows need not be diffusive. In fact, non-diffusive behavior in steep density gradients, as near the sharp subshock transition and at an upstream free escape boundary, is critically important for all aspects of particle acceleration and MFA. Henceforth we use Fermi acceleration to include all cases including those where diffusive behavior does dominate.

γ -ray spectra well below 100 TeV (e.g., Funk 2015). These remnants have been observed with the currently operating ground-based Cherenkov telescopes *H.E.S.S.*, *MAGIC* and *VERITAS*.

We note that there is an unidentified diffuse H.E.S.S. source in the Galactic Center (GC) region (i.e., HESS Collaboration et al. 2016) with no clear spectral break or cut-off until tens of TeV and this may well be a PeV CR accelerator. There are a number of possible interpretations of this γ -ray source. The Pevatron can be associated with the massive black hole Sgr A* (e.g., Aharonian & Neronov 2005, Fujita et al. 2017, Guo et al. 2017) which may produce a blast wave after a tidal disruption event to accelerate particles (e.g., Liu et al. 2016). An alternative explanation is that a supernova exploded close to the GC and interacted with either the fast wind from the GC or with a wind from its parent compact cluster of massive stars. We will discuss such a “colliding shock flow system” later in this paper and give estimates of the maximum CR energies achievable at very different evolution stages and for different types of SNe, as well as the possible role superbubbles play (Bykov 2001, Parizot et al. 2004, Ferrand & Marcowith 2010, Ackermann et al. 2011, Bykov 2014, Ohm 2016).

The review lay out is as follows. In §2 we detail the observational status of particle acceleration in SNe and in SNRs. In §3 we discuss CR acceleration beyond the PeV regime by trans-relativistic SNe or in superluminous SNe. In §4 we describe the different ingredients relevant for the investigation of particle acceleration in fast SN shocks as well as the expected radiation spectra produced at fast shocks. Section 5 discusses other galactic sources of PeV-EeV CRs: superbubbles and SNe in clusters. Section 6 addresses future observational facilities which should result in a substantial improvement in our understanding of CR acceleration in SNe.

2 Observational status

In this section we discuss some observations of SNe. In Section 2.1 we consider mainly radio observations of extragalactic SNe where the SN explosion and its immediate aftermath can be observed. In Section 2.2 we consider evidence for MFA from galactic SNRs where detailed observations can be made from radio to γ -rays.

2.1 Radio supernovæ

Today about 200 extragalactic SNe have been detected in radio, but only seven are sufficiently close to show well-resolved light curves at radio wavebands. These are SN 1979C (SN IIL), SN 1986J (SN IIn), SN 1987A (SN Ipec), SN 1993J (SN I Ib), SN1996cr (SN IIn), SN 2008iz, and SN 2011dh (SN I Ib) (Bartel et al. 2017, and references therein), where the type of the core-collapse SN has been added in parenthesis when available. Among the objects in this list we discard SN 1987A and SN 1996cr. The former shows peculiar behavior difficult to account for in the following simplified models and the latter does not have enough data to constrain the shock dynamics and magnetic fields. Considering type Ib/c SNe, we have selected the following objects on the basis of the amount of radio data available: SN 1983N, SN 1994I, SN 2003L (Weiler et al. 1986, Soderberg et al. 2005), and discuss the case of SN 2009bb since it is a relativistic Ibc SN (Soderberg et al. 2010) (see also §3.1).

Radio emission is due to synchrotron radiation from electrons accelerated by turbulent magnetic fields which develop in a region including both reverse and forward shocks. However, the exact nature of these turbulent magnetic fields, and the exact region of acceleration, remain elusive (Björnsson & Keshavarzi 2017). There are different locations where such turbulent magnetic fields can develop: at the contact discontinuity where Rayleigh-Taylor instabilities develop with fingers of the ejecta stretching into the shocked circumstellar medium (CSM), and/or at the forward or reverse shock where existing turbulence can be amplified and the acceleration of CRs in high-speed shocks can drive new MFA. Modeling of the radio lightcurves in different wavebands requires accounting for a number of processes. These include synchrotron self-absorption (SSA), free-free absorption by the ambient thermal plasma

Name	α	t_0 (days)	$([B_0(\text{G})], n)$	$(R_0(\text{cm}), m)$
SN 1979C	$0.74^{+0.05}_{-0.08}$	5	$([20 - 30], -1.00)$	$(8.68(e14), 0.91 \pm 0.09)$
SN 1986J	$0.67^{+0.04}_{-0.08}$	5	$([30 - 50], -1.00)$	$(3.18(e15), 0.69 \pm 0.03)$
SN 1993J	1.00	10	$([25.5], -0.93 \pm 0.08)$	$(1.9(e15), 1.00)$
...	0.90	100	$([2.4 \pm 1.0], -1.16 \pm 0.20)$	$(1.6(e16), 0.829 \pm 0.005)$
SN 2008iz	1.00	100	$([0.2 - 1.5], -1.00)$	$(2.1(e16), 0.86 \pm 0.02)$
SN 2011dh	1.15	4	$([5.9], -1.00 \pm 0.12)$	$(5.0(e14), 1.14 \pm 0.24)$
...	0.95	15	$([1.1], -1.00)$	$(3.1(e15), 0.87 \pm 0.07)$

Table 1 Magnetic field and shock radius evolution in a set of type II SNe. The spectral index α corresponds to the optically thin synchrotron spectrum. Estimations for SN 1979C and SN 1986J are based on a SSA model. Magnetic field strengths are derived at day 5 and are compatible with the strength of equipartition magnetic field given in Martí-Vidal et al. (2011). The value for n is obtained from the solution of propagation in a wind with constant mass loss rate with $s = 2$ (see Eq. 1). SN 1993J: Fransson & Björnsson (1998) use an expansion index $m = 0.74$ at $t > 100$ days, Martí-Vidal et al. (2011) present a long term radio survey where the expansion law index at frequencies above 1.7 GHz varies from $m \leq 0.925 \pm 0.016$ before $t_{\text{br}} = 360 \pm 50$ days to $m \geq 0.87 \pm 0.02$ after. SN2008iz: Kimani et al. (2016) derive the equipartition magnetic field strength, the lower and upper solutions depend if protons are not or are accounted in the estimation. References: Weiler et al. (1991), Marcaide et al. (2009), Martí-Vidal et al. (2011) for SN 1979C, Weiler et al. (1990), Bietenholz et al. (2010), Martí-Vidal et al. (2011) for SN 1986J, Fransson & Björnsson (1998), Tatischeff (2009) for SN 1993J, Kimani et al. (2016) for SN 2008iz, Horesh et al. (2013), Krauss et al. (2012), Yadav et al. (2016) for SN 2011dh.

(an internal effect) or by CSM matter (an external effect), and possibly plasma processes like the Razin-Tsyтович effect (Fransson & Björnsson 1998).

Radio observations are important for understanding many aspects of particle acceleration. First, the spectral turnover produced by SSA leads to an estimate of the magnetic field intensity of the synchrotron emitting zone. Second, the synchrotron spectral index provides a constraint on the electron distribution function and then on the acceleration process. Third, radio images are used to derive the SN shell dynamics, time evolution of the shock radius and its velocity, both quantities mandatory for any microphysical calculation of particle acceleration efficiency (e.g., Tatischeff 2009). The shell radius and speed can also be compared to a self-similar expansion model (e.g., Chevalier 1982).

The properties of the radio emission depend on the SN type: type Ib/c SNe show steep spectral indices ($\alpha > 1$, with a radio flux scaling as $S_\nu \propto \nu^{-\alpha}$), and have similar flux peaking before optical maximum at a wavelength around 6 cm, while other type II SNe show flatter spectra ($\alpha < 1$) with a wider range of radio luminosities usually peaking at 6 cm significantly after optical maximum (e.g., Weiler et al. 2002). Björnsson & Keshavarzi (2017) suggested that the radio emission in type Ib/c SNe comes from a narrow region in the vicinity of the forward shock, while the radio emission region of type IIb SNe (e.g. SN 1993J) is wider due to the effect of the RayleighTaylor instability.

In tables 1 and 2 we summarize the main properties of the above SNe from the available data deduced from VLBI observations. In addition to α , we use the following notation. The magnetic field strength is characterized by its amplitude B_0 at a reference time t_0 to be specified and the spectral index $n > 0$ of its time variation: $B(t) = B_0(t/t_0)^{-n}$. The VLBI shell radius is characterized by its radius at t_0 , R_0 and by the index $m > 0$ of its time variation: $R_{\text{sh}} = R_0(t/t_0)^m$. The shell velocity can then be deduced by $V_{\text{sh}} = dR_{\text{sh}}/dt$. Notice that the time evolution of the magnetic field is proportional to the energy density in the shock as described by Martí-Vidal et al. (2011)

$$B \propto \rho V_{\text{sh}}^2 \propto t^{m \frac{2-s}{2} - 1} . \quad (1)$$

Here the mass density profile of the pre-SN stellar wind is assumed to be $\rho \propto r^{-s}$. In the case of a shock propagating in a wind profile with a constant mass loss rate, that is with $s = 2$, we find from Eq. (1) an index for the magnetic field dependence of $n = 1$.

What is obvious from these tables is that the magnetic field quite early in the SN evolution is, in general, far in excess of critical magnetic field strengths obtained by balancing magnetic and wind kinetic energies (e.g., ud-Doula & Owocki 2002). The critical magnetic field is given by $B_{\text{cr}}^2/8\pi = \rho v_w^2/2$, where v_w is the stellar wind speed of the massive star. A general value

Name	α	$t_0(\text{days})$	$(B_0(\text{G}), n)$	$(R_0(\text{cm}), m)$
SN 1983N	1.03 ± 0.06	13	(3.6, -1.00?)	(2.3(<i>e</i> 15), 0.81)
SN 1994I	1.22	10.125	(2.3, -)	(2.39(<i>e</i> 15), -)
SN 2003L	1.1	10	(4.5, -1.00)	(4.30(<i>e</i> 15), 0.96)
SN 2009bb	1.0	20	(0.6, -1.00)	(3.20(<i>e</i> 16), 1.00)

Table 2 Magnetic field and shock radius evolution in a set of type Ib/Ic SNe. In the case of SN 1983N, the magnetic field strength dependence with time is assumed, Slysh (1992) only derives estimates of an upstream magnetic field strength of 0.9 G which is multiplied by 4 here. In the case of SN 1994I, the fitted parameters of the model derived by Alexander et al. (2015) do not show a simple power-law time dependence for both B and R . References: Weiler et al. (1986), Slysh (1992) for SN 1983N, Weiler et al. (2011), Alexander et al. (2015) for SN 1994I, Soderberg et al. (2005) for SN 2003L, Soderberg et al. (2010), Chakraborti & Ray (2011) for SN 2009bb.

in Gauss is

$$B_{\text{w,eq,G}}(t) \simeq \left[\frac{2.5 \times 10^{13}}{R_0} \right] \dot{M}_{-5}^{1/2} V_{\text{w},10}^{1/2} \left(\frac{t}{t_0} \right)^{-ms/2}, \quad (2)$$

where the stellar mass loss rate is in units of $10^{-5} M_{\odot}/\text{yr}$ and the wind speed is in units of 10 km/s. For the case of a red supergiant wind where the pre-SN mass loss rate $\dot{M}_{-5} \sim 1$, $V_{\text{w},10} \sim 1$, and $R_0 \sim 10^{15}$ cm, field strengths of the order of 25 mG are obtained, far below those shown in the tables. It requires $V_{\text{w}} > 1000$ km/s and high mass loss rates to find $B_{\text{eq}} \sim$ Gauss, which may be the case in some WR winds. In general, however, amplification factors of two to three orders of magnitude above B_{eq} are deduced from radio observations.

Recently, Kundu et al. (2017) discussed possible constraints on the circumstellar medium from the radio non-detection of two Type Ia supernovae, SN 2011fe and SN 2014J. They found a very low-density medium around both the SNe assuming that about 20% of the shock bulk energy was shared equally between electrons and magnetic fields. Note that the non-linear DSA modeling by Bykov et al. (2014) predicted about 10% efficiency of non-adiabatic magnetic field amplification by CR-driven instabilities (see Fig. 6 below), while the electron acceleration efficiency is usually lower.

As already mentioned, the physical processes producing magnetic field amplification are not fully understood. The possibility that CR driven plasma instabilities can produce this amplification is discussed below and we refer to Tatischeff (2009) and Marcowith et al. (2014) for additional work. Before providing more details on the CR instabilities we now briefly review the observational evidence that such instabilities develop in more evolved SNRs.

2.2 Supernova remnants

Supernova remnants are known sites of particle acceleration as they produce non-thermal radiation from radio to γ -rays (see Marcowith et al. 2016, for a review). Associated with this particle acceleration is clear evidence of magnetic field amplification in all historical SNRs making it likely that the two processes are tightly linked (e.g., Parizot et al. 2006).

The most direct evidence for MFA comes from high angular resolution observations of nonthermal X-rays. The *Chandra* X-ray satellite has detected in historical SNRs, in the hard 4–6 keV band, thin filaments of typical size 1-10% of the remnant radius. Such X-ray emission can hardly be interpreted as Bremsstrahlung radiation from relativistic electrons as it would require a very high ambient ISM density (Ballet 2006). Hence, this radiation is interpreted as synchrotron emission produced by multi-TeV electrons. The size of the filaments puts some constraints on the post-shock magnetic field intensity: electrons downstream from the shock are transported either diffusively or are advected with the flow but can radiate X-rays only within a synchrotron loss timescale. Since both the diffusion coefficient and the synchrotron loss time depend on the magnetic field intensity the radiation zone is limited. Typical field strengths between 50 (in older SNR like SN 1006) and 500 μG (in younger SNRs like Cassiopeia A) are deduced by this technique (Parizot et al. 2006). In fact, since *Chandra* has a finite point spread function, the deduced magnetic field intensity is only a lower limit in some cases.

Lately, *Chandra* has detected regularly spaced stripes in the X-ray synchrotron emission from Tycho's SNR (Eriksen et al. 2011). This pattern and spacing has been interpreted by Bykov et al. (2011) as a signature of magnetic turbulence produced by the short-scale Bell instability driven by PeV CR protons. However, recent observations by VERITAS and Fermi (i.e., Archambault et al. 2017) suggest that the proton spectrum may be cutting off well below PeV energies. If the stripes are, in fact, the result of CR-driven turbulence, the turbulence may result from the long-wavelength mirror instability driven by CRs undergoing super-diffusion (i.e., Lévy flight; see § 3.1) (Bykov et al. 2017b). The turbulence resulting from the mirror instability will have characteristic wavelengths long compared to the CR gyroradius, in contrast to the shorter wavelength turbulence produced by the Bell instability.

An important observational perspective would be to identify filaments at other wavelengths to constrain the MFA process. The improved sensitivity at 1 GHz of the *Square Kilometer Array* (SKA) (see § 6.1), with less than an arcsecond angular resolution, could bring some strong constraints on radio filaments and radio precursors (e.g., Achterberg et al. 1994).

Supernova remnants are also strong γ -ray emitters. This γ -ray emission can be of leptonic origin, i.e., inverse-Compton (IC) or bremsstrahlung radiation in dense environments, or hadronic, i.e., pion-decay. A trend seems to appear as a function of the remnant age (Acero et al. 2015, 2016). Young (with an age < 1000 yr) SNRs usually show hard spectra with a photon index close to 2 whereas older SNRs exhibit soft spectra beyond GeV energies. The γ -ray spectra of young SNRs can be interpreted within the framework of one-zone models as being produced by IC radiation. But from X-ray observations we know that in SNRs where MFA is occurring (see above), a one zone description of acceleration and cooling is likely a poor approximation since the magnetic field will vary behind the forward shock (Marcowith & Casse 2010). Also, if SNRs propagate into the perturbed ISM or CSM, density inhomogeneities can boost γ -ray emission from pion-decay forcing multi-zone models (Gabici & Aharonian 2014).

In the few young core-collapse SNRs which are γ -ray emitters (e.g., Cassiopeia A, RX J0852.0-4622), the γ -ray spectrum seems to cut off around 10 TeV implying a CR spectrum cutting off below ~ 100 TeV. For the moment there are no hints of a source of PeV CRs which would then produce pion-decay γ -rays of ~ 300 TeV. Older SNRs show a cut off below one TeV. One possibility is that the Pevatron phase is very short after the SN outburst and ends before an age of ~ 1000 yr. This question is treated in the next section.

3 CR acceleration beyond PeV

Observations of the spectrum, composition, and anisotropy of CRs below the knee were briefly mentioned in §1 (see also Hillas 2005). An important question that is yet to have a definitive answer for higher energy CRs is where the transition between the galactic and extragalactic CR components occurs. It is even possible that the spectral breaks that have been observed below PeV energies, combined with the light-mass CR component between $10^{17} - 10^{18}$ eV suggested by *LOFAR* observations, may indicate the presence of different types of galactic sources which have not been previously considered.

While providing a sufficient energy budget is the most important constraint for sources of GeV-TeV CRs, the energy content in CRs beyond the knee is considerably less. This opens the possibility these CRs may be produced by low-power sources or by rare powerful events. Of course SNe are still among the possible sources of high-energy galactic CRs and Sveshnikova (2003) discussed the role the diversity in supernova explosion energies might have on CR spectral features around the knee. In particular, PeV CRs may be produced by a subset of type Ibc SNe with trans-relativistic shocks (e.g., Budnik et al. 2008, Chakraborti et al. 2011, Ellison et al. 2013), or by superluminous SNe (e.g., Murase et al. 2011, 2014, Zirakashvili & Ptuskin 2016), or by SNe in young compact stellar clusters (Bykov 2014, Bykov et al. 2017a). We shall now briefly discuss these sources.

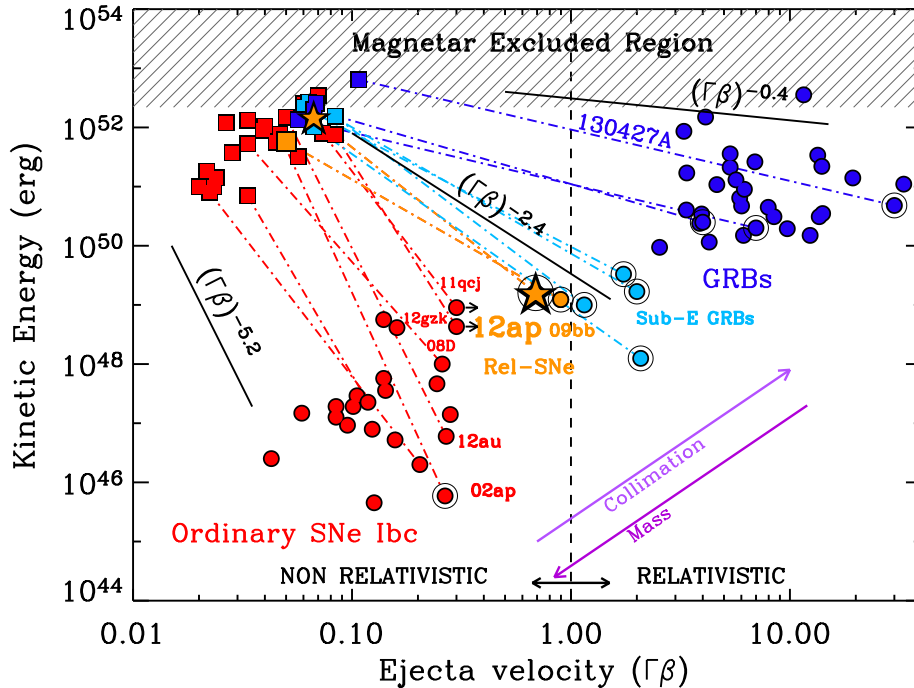


Fig. 1 The kinetic energy of the ejecta as a function of the spatial component of the ejecta four velocity $\Gamma\beta$ is shown for distinct classes of core collapsed events: ordinary type Ibc SNe (red), GRBs (blue), sub-energetic GRBs (light-blue), and relativistic supernovae SN 2009bb and SN 2012ap (orange). Adapted from Margutti et al. (2014).

3.1 CR acceleration in trans-relativistic supernovae

Soon after the cosmological nature of γ -ray bursts was established an unusually radio bright supernova SN1998bw was associated with GRB980425. This SN showed clear evidence for a blast wave moving at relativistic speeds (e.g., Kulkarni et al. 1998). The mass in the relativistic ejecta of SN1998bw was estimated as $M_{\text{ej}} \sim 10^{-5} M_{\odot}$, with the energy in the relativistic outflow $\gtrsim 10^{49}$ erg. There are also indications for the existence of relativistic SNe without a detected GRB. The rare subclass of type Ibc SNe is distinguished from ordinary SNe by the presence of ejecta moving at mildly relativistic speeds (e.g., Soderberg et al. 2006). In Fig. 1 (adapted from Margutti et al. 2014) the kinetic energy of the ejecta as a function of the spatial component of the ejecta four velocity is shown for distinct classes of core collapsed events: ordinary type Ibc SNe (red), GRBs (blue), sub-E GRBs (i.e., sub-energetic; light-blue), and the relativistic supernovae SN 2009bb and SN 2012ap (orange). The events lying near the $\Gamma\beta = 1$ line represent a subset of SNe with mildly relativistic ejecta speeds and other properties intermediate between ordinary SNe and GRBs.

A prototype of a relativistic SNe without a detected GRB is SN 2009bb (Soderberg et al. 2010, Margutti et al. 2014). In this remnant, radio observations were used to probe the fastest ejecta as the expanding relativistic blast wave propagated through the fast wind of the progenitor star. In the case of SN 2009bb, Soderberg et al. (2010) estimated that the ejecta had a minimum energy of $(1.3 \pm 0.1) \times 10^{49}$ erg, with a Lorentz factor $\Gamma \simeq 1.3$ (see Fig. 1), and were propagating in the wind of the progenitor star with an estimated mass loss rate of $\dot{M} = (2 \pm 0.2) \times 10^{-6} M_{\odot} \text{ yr}^{-1}$.

A simple estimate of the deceleration length, R_s , of a SN shock assuming the ejected mass, M_{ej} , equals the amount of swept up mass in a progenitor wind with speed v_w and mass loss rate \dot{M} is

$$R_s \approx 10^{17} \left[\frac{M_{\text{ej}}}{10^{-5} M_{\odot}} \right] \left[\frac{v_w}{3 \times 10^3 \text{ km s}^{-1}} \right] \left[\frac{10^{-6} M_{\odot} \text{ yr}^{-1}}{\dot{M}} \right] \text{ cm} . \quad (3)$$

The stellar wind mass-loss rate of $10^{-6} M_{\odot} \text{ yr}^{-1}$, and the wind terminal speed of 3000 km s^{-1} , are consistent with predictions for the He main sequence stars which were presented recently by Vink (2017), while the Wolf-Rayet type stars collected by Nugis & Lamers (2000) demonstrated somewhat higher mass-loss rates and lower wind velocities. The values and configurations of the magnetic fields in the winds of the potential progenitors are not very certain (e.g., Walder et al. 2012), while the analysis of radio observations of SN2009bb (Chakraborti et al. 2011) revealed a magnetic field of $\gtrsim 0.1 \text{ G}$ at the estimated radius of $\gtrsim 10^{17} \text{ cm}$ (see their Figure 1 for more details).

It is important to note that in a relativistic SN, both the shock speed and magnetic field in the wind of the progenitor star are expected to be much higher than in the ISM. This will strongly reduce the acceleration time of particles subject to Fermi acceleration and may make it possible to accelerate nuclei well beyond PeV energies in a few months.

Budnik et al. (2008) estimated the conditions for Fermi acceleration in trans-relativistic SNe and concluded that the estimated rate and energy production by these sources are high enough to allow them to power CRs with energies up to 10^{18} eV . They assumed that the magnetic field is amplified by the shock both in the upstream and downstream regions to values close to equipartition. Moreover, Chakraborti et al. (2011) argued that relativistic SNe similar to SN 2009bb could be the sources of ultra-high-energy-cosmic-rays (UHECRs) with energies beyond the Greisen-Zatsepin-Kuzmin limit (i.e., $\gtrsim 10^{20} \text{ eV}$) if they have magnetic fields above $\sim 0.1 \text{ G}$ at radii beyond $\sim 10^{17} \text{ cm}$.

Of course relativistic SNe are scarce. The Chakraborti et al. (2011) conjecture was made assuming that the type Ibc SN rate is $\sim 1.7 \times 10^4 \text{ Gpc}^{-3} \text{ yr}^{-1}$ and the fraction of these which are mildly relativistic is $\sim 0.7\%$ (the uncertainty is large, however, $0.7_{-0.6}^{+1.6}\%$, or $(0.1 - 2.3)\%$). If the fraction 0.7% is right then one would expect a few trans-relativistic SNe occurring within a distance of a few hundred Mpc every year, and one every $5 \times 10^4 \text{ yr}$ in the Milky Way. A crucial point in these CR energy estimates is the magnetic field strength. Strong MFA is simply assumed but this must be justified by self-consistent models for MFA in nonlinear Fermi acceleration in trans-relativistic shocks.

Relativistic SNe may provide a distinct component of CRs beyond PeV energies. Supernova statistics in a volume-limited sample based on nearby SN rates from the Lick Observatory Supernova Search (Li et al. 2011) found that the most abundant type of SNe are type II (57% of the total), while type Ibc comprised about 19%, a fraction similar to that of SNe Ia which is estimated as 24%.

If indeed relativistic SNe are just 0.7% of all type Ibc SNe, as suggested by Soderberg et al. (2010) and Chakraborti et al. (2011), than their rate in the Galaxy is about one every $5 \times 10^4 \text{ yr}$. The diffusion coefficient D required for the high energy CRs to be confined in the Galactic halo of size R for $5 \times 10^4 \text{ yr}$ can be estimated to be $D \sim 2 \times 10^{31} (R/3 \text{ kpc})^2 \text{ cm}^2 \text{ s}^{-1}$. Note that the gyroradius of a proton of energy 10^{18} eV in the typical interstellar magnetic field is $\sim 10^{21} \text{ cm}$ providing a minimum value for $D \sim 10^{31} \text{ cm}^2 \text{ s}^{-1}$. The minimum value was derived assuming Bohm diffusion where the CR mean-free-path is equal to the gyroradius, however, the diffusion coefficient in the halo is expected to be well above the minimal value. This value, and the 2% upper limit on the anisotropy of $\sim 10^{18} \text{ eV}$ CRs (see Ptuskin 2012, for a discussion), requires an extended CR halo of size $\sim 10 \text{ kpc}$ if the relativistic SNe are to be the dominant source of CRs up to $\sim 10^{18} \text{ eV}$. The CR-driven galactic winds (e.g., Farber et al. 2017, Recchia et al. 2017, and references therein) may affect the scale size R of the CR confinement region. The power required to maintain this high-energy galactic CR component (assuming it is quasi-steady) is about $10^{36} \text{ erg s}^{-1}$ meaning trans-relativistic shocks would need to place $\sim 10\%$ of the mildly relativistic outflow kinetic energy into CRs extending to 10^{18} eV . It has also been suggested by Loeb & Waxman (2006) that relativistic SNe may produce high-energy CRs in starburst galaxies and be a source of high-energy neutrinos.

The UHECRs with energies well above 10^{18} eV are most probably of extragalactic origin. The main source candidates are γ -ray bursts and powerful radio-galaxies. Galactic magnetars may also contribute. In all cases, high power and relativistic outflows are required to produce the most extreme CR energies (e.g., Waxman 1995, Blasi et al. 2000, Arons 2003, Lemoine 2013, Asano & Mészáros 2016).

To address MFA with high CR acceleration efficiency in trans-relativistic shocks we generalize a Monte Carlo technique that has been used previously to study nonlinear Fermi acceleration in shocks of all Lorentz factors but without a self-consistent calculation of MFA in relativistic flows (Ellison et al. 2013, Warren et al. 2015, 2017). This previous model assumed a given structure for the magnetic turbulence which was not directly determined by the CR distribution. While neglecting MFA in relativistic shocks might be acceptable if Fermi acceleration is inefficient, the efficiency estimate given above suggests that Fermi acceleration is efficient enough in trans-relativistic shocks to produce CR pressure gradients and CR currents strong enough to drive instabilities responsible for MFA in a way similar to what is believed to occur in non-relativistic shocks (e.g., Bell & Lucek 2001, Bell 2004, Bell et al. 2013, Schure et al. 2012, Bykov et al. 2013, Marcowith et al. 2016, Bykov et al. 2017b, van Marle et al. 2017).

The non-relativistic Monte Carlo simulation self-consistently finds a steady-state, planar-shock solution for the nonlinear shock structure including (1) injection of particles from the thermal background, (2) modification of the precursor flow by energetic particle and magnetic field pressure, (3) calculation of the magnetic turbulence (i.e., MFA) due to the anisotropic distribution of the accelerated particles, (4) turbulence cascade, (5) a determination of the momentum and space dependent scattering mean free path from the self-generated turbulence, (6) a self-consistent calculation of the scattering center speed³ (which may model an effect of a mean electric field in the shock upstream) without reference to the Alfvén velocity, and (7) particle escape at an upstream free escape boundary. Most recently (i.e., Bykov et al. 2014, 2017b), super-diffusion (also called *Lévy-walk* or *Lévy-flight* propagation) has been included within the full nonlinear code structure.

In contrast to PIC simulations, where the magnetic turbulence is determined directly from particle motion using Maxwell’s equations, the Monte Carlo code calculates the resonant and non-resonant instabilities by coupling analytic descriptions of the growth rates with the anisotropic particle transport simulated by the code. In Fig. 2 we show preliminary results from our trans-relativistic code.

The figure shows spectra of magnetic fluctuations for Lorentz factors between 1.5 and 4 assuming no turbulence cascade along the initial magnetic field (c.f., Lithwick & Goldreich 2001). The turbulence was calculated self-consistently with the CR distributions shown in Fig. 3. It is critical to note that, for clarity, Figs. 2 and 3 only show spectra for the downstream region (the particle distributions are calculated in the shock-rest frame). There is no strict one-to-one correspondence between the CRs and the turbulence in these plots. All spectra are calculated throughout the shock precursor with the convection of turbulence and CRs taken into account. The turbulence shown in Fig. 2 is the net result, in the downstream region, of production, convection, and cascading, if present.

The effect of strong magnetic field amplification is clearly seen in Fig. 2. The self-generated turbulence stands more than an order of magnitude above the background level (dashed black curve) for all wavenumbers and Lorentz factors. In addition, there is much stronger amplification of long-wavelength turbulence (i.e., $k \sim 10^{-6} r_{g0}^{-1}$) produced by CRs that escape at the upstream FEB. The quasi-thermal CRs also produce enhanced turbulence for $k \sim 10 - 100 r_{g0}^{-1}$.⁴ While not shown, we have performed these calculations with Kolmogorov-type cascade and found little difference in the particle spectra or the total value of the amplified magnetic field. The background turbulent magnetic field in the wind of the progenitor star (dashed line in Fig. 2), integrated over the spectrum, had a magnitude $B_{\text{turb}} \sim 0.01$ G for these simulations. This is considerably less than the shock ram pressure and the amplified turbulent magnetic field in the shock downstream which is ~ 0.2 G. The wind of the WR type progenitor star with the magnetic field value ~ 0.01 G at $R \sim 10^{17}$ cm is magnetized if the mass-loss rate is $\sim 10^{-6} M_{\odot} \text{ yr}^{-1}$.

³ See Fiorito et al. (1990) for an early calculation of the scattering center speed using Monte Carlo methods.

⁴ Particle-particle interactions, i.e., Coulomb collisions, are not explicitly modeled in the Monte Carlo simulation so true thermal distributions are not produced. Therefore, we use the term “quasi-thermal” to describe the peaks at thermal energies seen in Fig. 3. These peaks have essentially the same mean and total energy as the equivalent Maxwell-Boltzmann distributions.

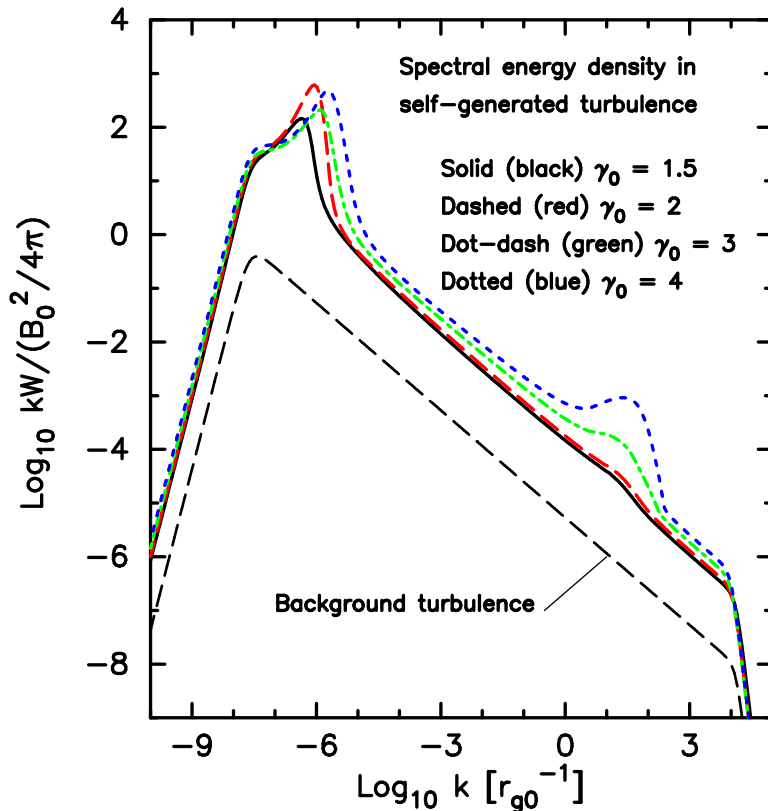


Fig. 2 Preliminary results showing spectral energy densities of the CR-driven magnetic fluctuations measured in the downstream region of trans-relativistic shocks with indicated Lorentz factors, γ_0 . The black dashed curve is the background turbulence. There is no turbulence cascade in this model (Bykov et al. 2017c).

We find, even for $\gamma_0 = 4$, that escaping CRs are important. In Fig. 4 we show distributions of escaping CRs as seen by a far upstream observer. These spectra are determined by

$$Q_{\text{esc}}(p) = -\frac{J_{\text{cr}}(z_{\text{FEB}}, p)p^4}{4\pi m_p c u_0}, \quad (4)$$

where u_0 is the shock speed and $J_{\text{cr}}(z_{\text{FEB}}, p)$ is the CR current, both measured in the far upstream rest frame. Here z_{FEB} is the position of the upstream FEB and for the plots shown, z_{FEB} was 3×10^{16} cm from the subshock at $z = 0$.

3.2 CR acceleration in interaction powered luminous supernovae

Superluminous SNe with a peak luminosity in the optical-UV of $\sim 10^{44}$ erg s^{-1} were recently recognized to be a broad class of events with the rate estimated to be $\sim 10^{-4}$ of the core-collapse SN rate (e.g., Branch & Wheeler 2017). The detected events were both hydrogen rich and hydrogen poor, while some of them were apparently dominated by radioactive ^{56}Ni decay (e.g., Gal-Yam 2012). A superluminous SN event may occur in the case of a dense enough circumstellar medium around the SN which provides a radiation-dominated shock propagating through the envelope (e.g., Falk & Arnett 1977, Chugai & Danziger 1994, Chevalier & Irwin 2011, Chevalier 2012, Blinnikov 2016b,a, Sorokina et al. 2016). Pre-supernova activity of a massive progenitor star during some evolutionary phases may have a very large mass-loss rate in the form of a dense slow wind that produces dense circumstellar envelopes (Smith 2017, Morozova et al. 2017). Multiple envelopes may be formed if outbursts occur at different progenitor star evolutionary stages prior to the SN event.

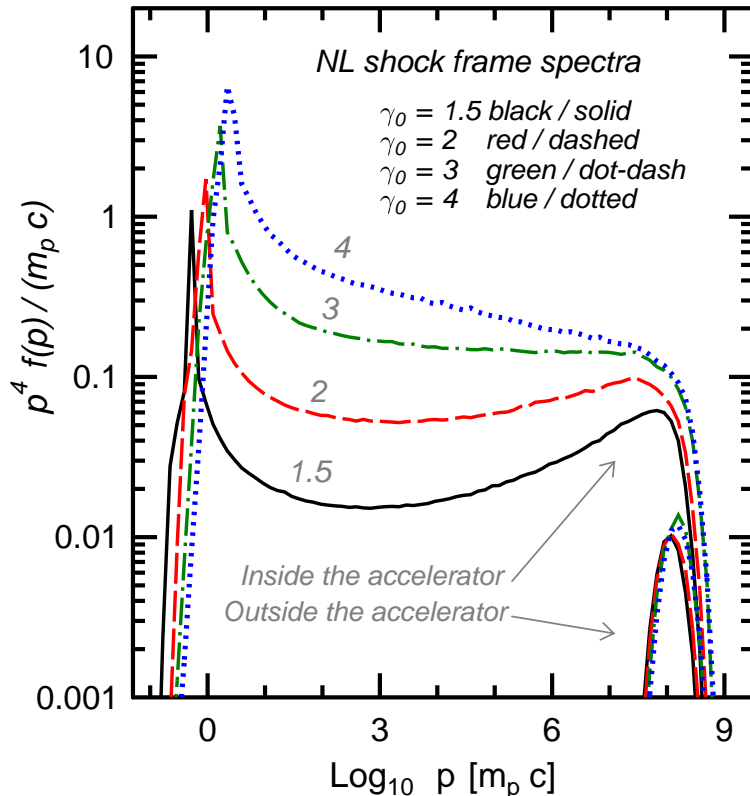


Fig. 3 Shown are proton phase-space distributions measured in the shock rest frame (preliminary results from Bykov et al. 2017c). These nonlinear, steady-state, Monte Carlo simulations were performed for the trans-relativistic shock Lorentz factors, γ_0 , indicated. The amplified magnetic turbulence determined self-consistently with these spectra is shown in Fig. 2.

Assuming that $\sim 10\%$ of the shock ram pressure can be converted to the fluctuating magnetic field (c.f. Fig. 6) and using the minimal Bohm diffusion coefficient of CRs in the amplified field, Zirakashvili & Ptuskin (2016) estimated the maximal energy of protons accelerated by the Fermi mechanism in type IIIn SNe to be

$$\frac{E_{\max}}{80 \text{ PeV}} \leq \frac{E_{\text{SN}}}{10^{52} \text{ erg}} \left(\frac{M_{\text{ej}}}{10 M_{\odot}} \right)^{-1} \left(\frac{v_w}{100 \text{ km s}^{-1}} \right)^{-0.5} \left(\frac{\dot{M}}{10^{-2} M_{\odot} \text{ yr}^{-1}} \right)^{0.5}. \quad (5)$$

This implies that hypernovae with ejected kinetic energies of $E_{\text{SN}} \sim 10^{52}$ erg can accelerate protons beyond PeV energies. To reproduce the observed light curves of the superluminous SN 2006gy, assuming that the supernova is powered by the collision of supernova ejecta with a dense circumstellar medium, Moriya et al. (2013) derived an ejecta mass $\lesssim 15 M_{\odot}$ and an explosion energy $\gtrsim 4 \times 10^{51}$ erg. Moriya & Maeda (2014), based on the observed rise times and peak luminosities in type IIIn SNe, found substantial diversity in their progenitor wind densities, SN ejecta energies, and ejecta masses.

The interactions of the accelerated CRs with the dense circumstellar envelope of the interaction powered SNe would result in rich multi-wavelength nonthermal emission, as well as

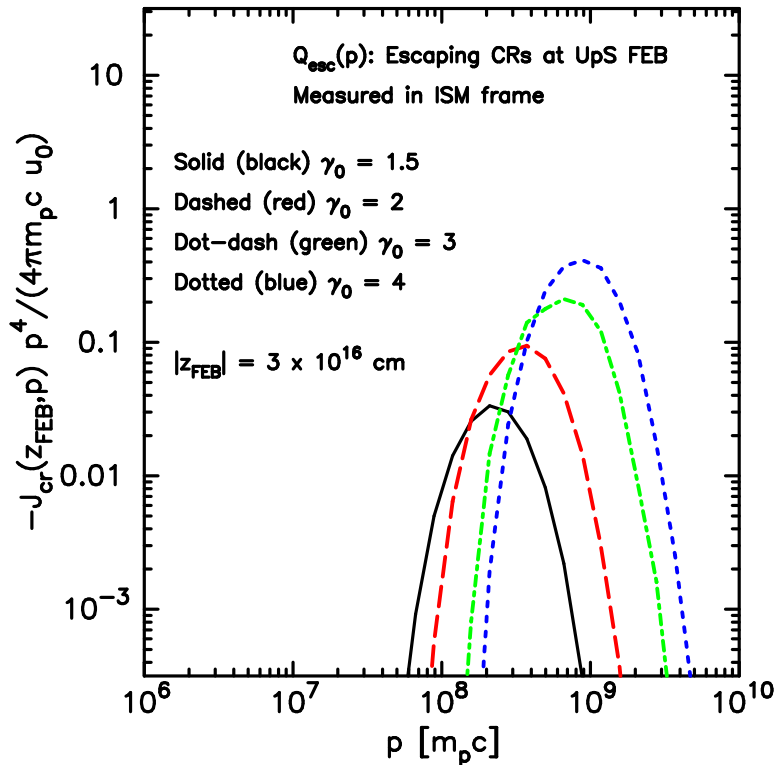


Fig. 4 Shown are distributions of protons escaping at the upstream free escape boundary (FEB) (i.e., Eq. 4), as measured in the far upstream (i.e., the ISM) rest frame. The trans-relativistic shock Lorentz factors are indicated. These are preliminary results from Bykov et al. (2017c).

high-energy neutrinos in the energy range of the *IceCube Observatory* (e.g., Katz et al. 2011, Murase et al. 2014, Zirakashvili & Ptuskin 2016, Petropoulou et al. 2017). The pp collisions between the accelerated CRs and the dense circumstellar envelope would efficiently produce γ -rays and neutrinos. Moreover, Murase et al. (2014) argued that secondary electrons and positrons, which are copiously produced in the inelastic pp collisions, radiate efficiently and would produce high-frequency synchrotron radio emission which could be observed by the *Jansky Very Large Array* and the *Atacama Large Millimeter/submillimetre Array* from type II_n SNe at Gpc distances. Petropoulou et al. (2017) estimated the diffuse neutrino emission from the SN II_n to be $\sim 10\%$ of the neutrino flux above 60 TeV observed by the *IceCube Observatory* (Aartsen et al. 2014). They also concluded that to produce the observed neutrino flux, the high-energy neutrino sources associated with type II_n events should comprise $\sim 4\%$ of all core collapse SNe and have a high-energy proton acceleration efficiency $> 20\%$.

4 Hydrodynamic models of evolving SNRs

An effective way to model the dynamic nature of SNRs is to couple the hydrodynamic evolution of the remnant with the CR production. A number of different models have been presented along these lines and we refer the reader to the original papers for details (e.g., Berezhko et al. 1996, Ellison et al. 2007, Kang et al. 2009, Telezhinsky et al. 2011, Ferrand et al. 2012, Lee et al. 2012, Brose et al. 2016). Supernovae and first-order Fermi shock acceleration have been actively studied for several decades and any reasonably consistent model of an evolving SNR producing CRs with an efficiency above 5 or 10% will be complex with a number of parameters and assumptions. In simplest terms, the different models combine various physical processes in a more or less self-consistent fashion. The important physical processes and model assumptions include:

4.1 Remnant geometry

Most models assume the SNR is spherically symmetric but multi-dimensional models (e.g., Ferrand et al. 2012) have been presented. Spherically symmetric models can include dense shells of material and mimic in an approximate fashion dense clumps of circumstellar material (e.g., Ellison & Bykov 2011). Multi-dimensional models are essential for modeling the irregular nature of many remnants and particularly those, such as SN1006, with clear asymmetries in emission (e.g., Cassam-Chenaï et al. 2008). Besides resulting from irregularities in the CSM, asymmetries, such as that seen in SN1006, may result from a varying shock geometry, as determined by the ambient magnetic field direction. Most theories of Fermi acceleration suggest that quasi-parallel shocks, those where the ambient magnetic field direction is nearly parallel to the shock normal, inject and accelerate CRs more efficiently than quasi-perpendicular shocks (e.g., Ellison et al. 1995). Observations and modeling of SN1006 (e.g., Rothenflug et al. 2004, Cassam-Chenaï et al. 2008) support this view.

4.2 Ejecta profile

The density of material ejected from the SN explosion is typically assumed to have a power law (e.g., Chevalier 1982) or exponential spatial distribution in radius (e.g., Dwarkadas & Chevalier 1998). A power law distribution, as assumed in Eq. (1), is amenable to self-similar solutions (e.g., Decourchelle et al. 2000) while an exponential distribution may be more appropriate for type Ia thermonuclear SNe. Of course, the ejecta distributions from actual SNe are likely to be more complex, as discussed in the next section.

4.3 Circumstellar material

The ejecta and outer blast wave will interact with the circumstellar medium adding another level of complexity (e.g., Raymond 2017). While type Ia SNe may explode in a uniform medium, core-collapse SNe are likely to explode in a more complex environment produced by pre-SN stellar winds (i.e., wind-blown bubbles) (e.g., Dwarkadas 2005), nearby dense molecular clouds, and/or colliding plasmas from nearby SNe and SNRs (e.g., Bykov et al. 2017a). If the SN blast wave interacts with dense external material, strong γ -ray emission from proton-proton interactions is expected as in SNRs W44, IC 443, and 3C 391 (see e.g. Tavani et al. 2010, Uchiyama et al. 2010, Abdo et al. 2010a,b, Ackermann et al. 2013a, Slane et al. 2015a). Recent work by Patnaude et al. (2017) has included ejecta profiles obtained from stellar evolution codes of core-collapse SNe and demonstrated that the mass-loss history leaves an imprint on X-ray emission lasting days to years after the collapse (see Fig. 5).

4.4 Production of a forward and reverse shock pair

In young SNRs the reverse shock will co-exist with the forward shock for a period of time and both will heat the thermal plasma to X-ray emitting temperatures and simultaneously produce CRs. Except for the extreme remnant limb, the observed line-of-sight will pass through material with very different parameters and shock histories. While single component models are often used, care must be taken to ensure the multi-component nature of the remnant is accurately accounted for. Interpreting the integrated multi-component emission in terms of simple power laws, as is often done, may be misleading.

4.5 Effect of CR acceleration on remnant dynamics, plasma heating, and thermal X-ray production

If CRs are produced efficiently (i.e., $> 10\%$ of the shock bulk flow kinetic energy is placed in relativistic particles), the backpressure of CRs will influence the remnant hydrodynamics

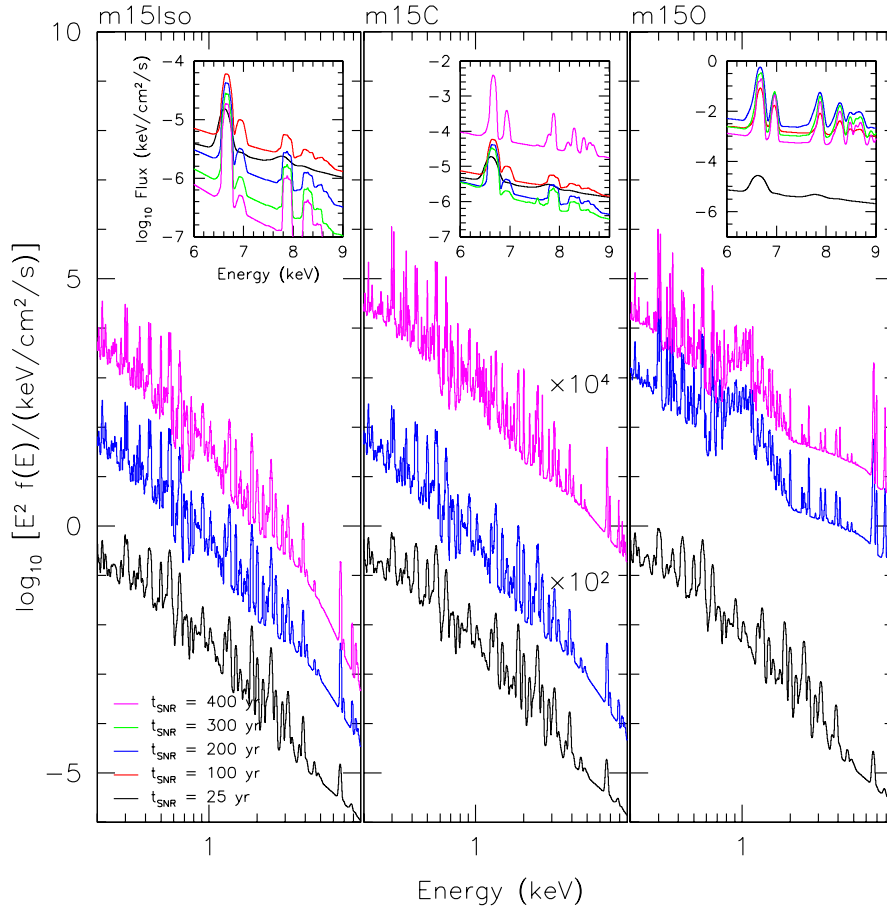


Fig. 5 Integrated X-ray spectra for three different end-to-end (i.e., pre-main sequence, through explosion, into the remnant phase) core-collapse SN models. In all panels X-ray spectra are plotted for different ages, as indicated by color. In the main panels, the spectra at 200 and 400 years are scaled relative to the spectra at 25 years. The inserts show absolutely normalized emission around the Fe-K line. This work shows that X-ray emission, even 100's of years after the explosion, differs noticeably depending on the progenitor mass-loss history and other details of the explosion. This is Fig. 8 from Patnaude et al. (2017) and this paper should be seen for details.

since relativistic particles produce less pressure for a given energy density than non-relativistic ones. The energy placed in CRs comes from the thermal plasma so the shocked temperature is less than expected for test-particle acceleration. Furthermore, the efficient production of CRs can result in an increase in the shock compression ratio from standard Rankine-Hugoniot values. The change in temperature and density of the shocked plasma will modify the X-ray line emission. This effect has been studied extensively with a code coupling the remnant hydrodynamics with efficient CR production (see Ellison et al. 2012, Patnaude et al. 2017, and references therein). The effect of CR production influences the non-equilibrium ionization X-ray emission in observable ways.

4.6 Magnetic field amplification (MFA)

The self-generation of magnetic turbulence is necessary for first-order Fermi shock acceleration to produce CRs to high energies. Beyond that, as shown in Section 2.1, it has become clear from observations of young SNRs that not only must turbulence be generated, it must be generated far more efficiently than envisioned when the Fermi mechanism was first proposed

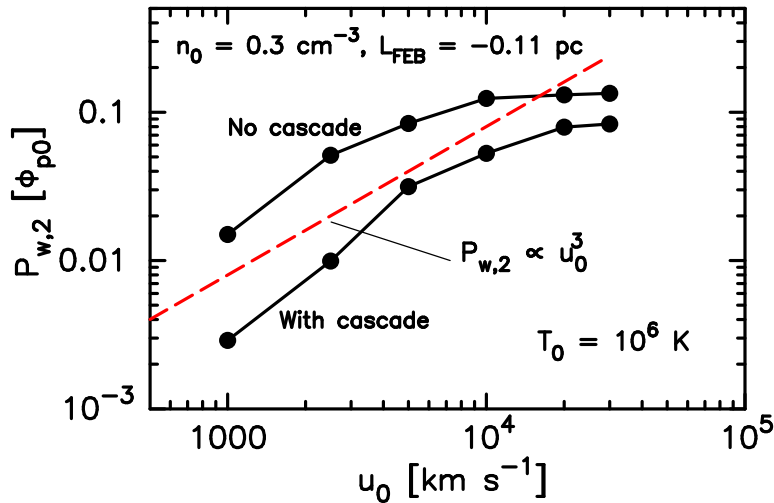


Fig. 6 The downstream pressure in magnetic fluctuations in units of the far upstream ram pressure vs. shock speed u_0 for various shock models simulated with a non-linear Monte Carlo model (see Bykov et al. 2014, for details). Models with and without turbulence cascade are included as indicated. The dashed (red) line approximates the behavior for low shock speeds. At higher speeds the turbulence saturates at the 10 – 15% level.

(e.g., Parizot et al. 2006). This MFA is strongly nonlinear and is generally added to hydro models in some approximate way. Obtaining self-consistent descriptions of MFA from both resonant and non-resonant instabilities is an active area of current research, as discussed in § 3.1.

In Fig. 6 we show figure 11 from Bykov et al. (2014) giving the pressure in magnetic turbulence versus shock speed u_0 , as obtained with Monte Carlo techniques including the resonant CR-streaming instability and two non-resonant CR-current instabilities (i.e., Bell 2005, Bykov et al. 2013). The Monte Carlo results show that the efficiency of MFA, as defined by the pressure in turbulence, saturates at $\sim 10 - 15\%$ of the far upstream bulk flow ram pressure.

4.7 Cosmic ray escape in Fermi acceleration

For the Fermi mechanism to work, particles must be confined to the shock by magnetic turbulence. The scale of this confinement is $\sim D(p)/u_{\text{sh}}$, where $D(p)$ is the diffusion coefficient of a CR with momentum p and u_{sh} is the shock velocity.⁵ Due to the self-generated turbulence, this diffusion coefficient is typically much smaller than that of the quiet ISM (e.g., Bell 1978, Lagage & Cesarsky 1983, Bell 2004), i.e., CR driven instabilities can provide amplification of the seed interstellar turbulence and, in some energy ranges, reduce the diffusion coefficient by orders of magnitude.

However, regardless of how efficient the MFA is, as long as the shock age is long compared to the acceleration time, there will always be some CR energy, determined by shock geometry, above which the accelerated particles can no longer generate enough turbulence to confine themselves to the shock. These high-energy particles will escape the accelerator while lower-energy CRs remain confined.⁶ If Fermi acceleration is efficient, the modified compression ratio for the highest energy CRs can become greater than four (see Berezhko & Ellison 1999) and the escaping energy flux can be a significant fraction of the total shock energy flux (see

⁵ Note that the far upstream shock speed is written as either u_0 or u_{sh} .

⁶ This assertion depends only on a diffusion coefficient which is an increasing function of CR momentum and the fact that all real shocks are finite in extent. In this case, at some p , $D(p)/u_{\text{sh}} \sim R_{\text{sh}}$, where R_{sh} is the shock radius, and the CR can no longer be confined independent of any plasma physics details (see Drury 2011, for a discussion of effects of the background ISM field).

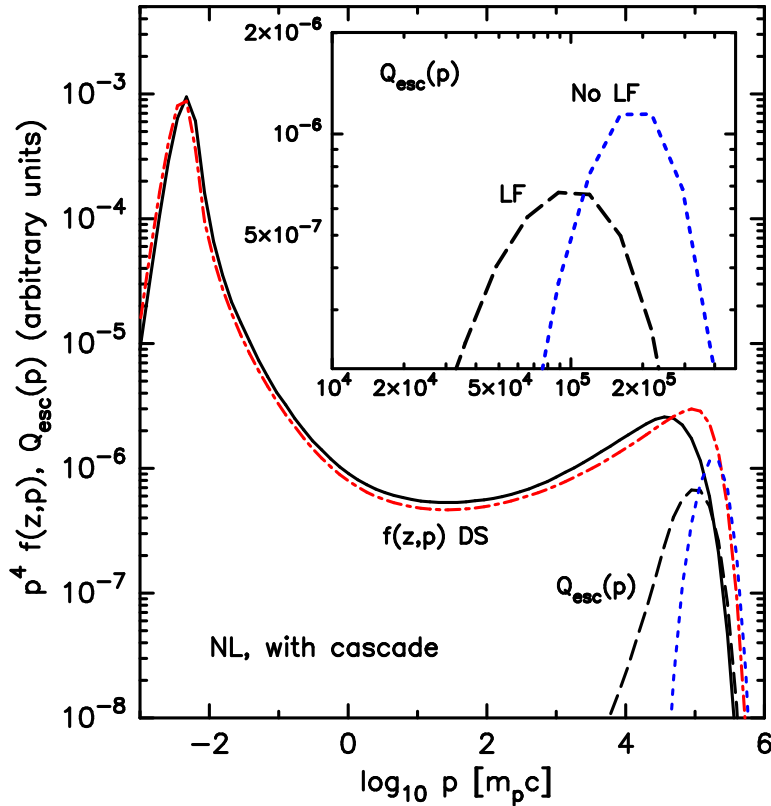


Fig. 7 Shown are proton phase-space distributions simulated with a nonlinear Monte Carlo model of superdiffusive shock acceleration (Bykov et al. 2017b). Downstream (DS) spectra, as well as the distributions of particles escaping the upstream FEB, are plotted. In the main panel, the black curves are with superdiffusion and the red and blue curves are with normal diffusion. The insert shows the escaping fluxes with superdiffusion (labeled ‘LF’) and with normal diffusion (labeled ‘No LF’). All spectra are absolutely normalized relative to each other.

Caprioli et al. 2009, Drury 2011, Ellison & Bykov 2011, Kang 2013, Malkov et al. 2013, for further discussion).

A consequence of escape is that, if SN shocks are producing galactic CRs by Fermi acceleration, an outside observer would see at each particular moment just a relatively narrow spectrum of the escaped particles centered at some maximum momentum $p_{\max}(t)$. However, since p_{\max} evolves with the SNR expansion, the time integrated CR spectrum can be an extended power law (e.g., Ptuskin & Zirakashvili 2005).

Basic Fermi acceleration assumes that fast particle transport in the shock precursor is described by standard diffusion due to particle scattering by magnetic turbulence. However, the transport of energetic particles in the presence of intermittent (i.e., non-Gaussian) magnetic turbulence produced by anisotropic CR distributions can be different from standard diffusion (see Zimbaro et al. 2015, for a recent review). This superdiffusive propagation (also called *Lévy-walk* or *Lévy-flight*) modifies the spectrum of escaping CRs. A nonlinear Monte Carlo model of Fermi acceleration with MFA, including superdiffusive transport in the shock precursor, has been presented by Bykov et al. (2017b). In Fig. 7 we illustrate the effect of superdiffusive particle transport on the shape of the spectrum of escaping CRs with superdiffusion (labeled ‘LF’) and without (labeled ‘No LF’). The escaping CR spectrum is clearly broadened when superdiffusion is taken into account. This broadening will influence the pion-decay emission and measurements of γ -ray spectra produced by CRs escaping a SNR adjacent to a molecular cloud can be used to constrain superdiffusive transport models.

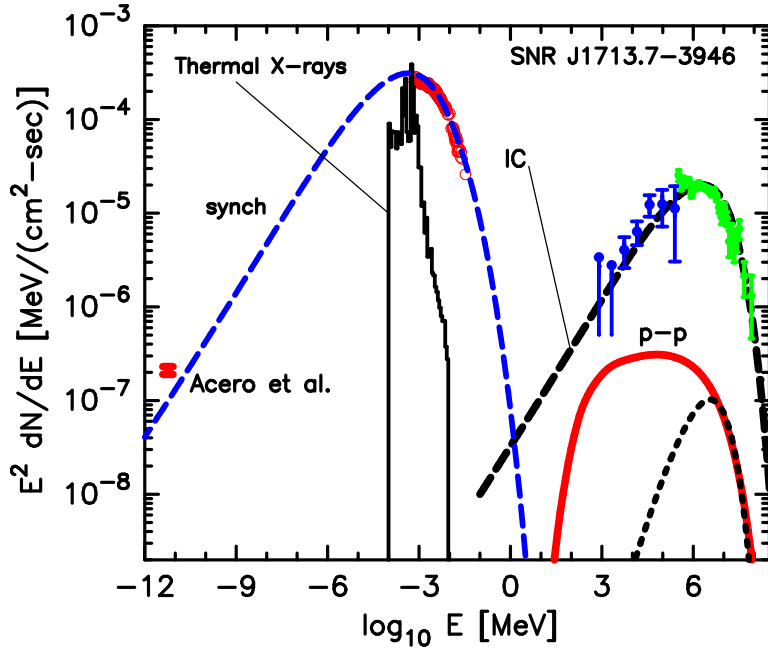


Fig. 8 Fit to SNR J1713 continuum and X-ray emission line observations. The different emission processes are indicated except the dotted black curve which is p-p emission from escaping CRs. This figure is adapted from figure 2 in Ellison et al. (2012) and that paper should be seen for details and references to the observations.

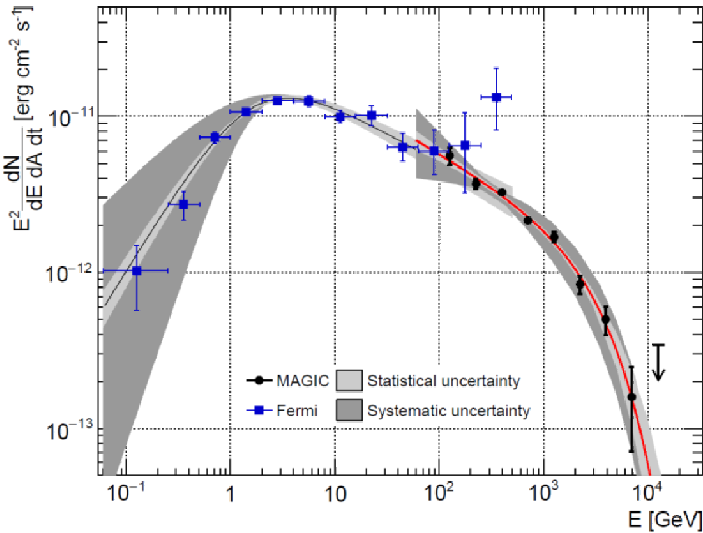


Fig. 9 Figure 1 from Ahnen et al. (2017) (“A cut-off in the TeV gamma-ray spectrum of the SNR Cassiopeia A”) showing the spectral energy distribution from the Cassiopeia A SNR. As indicated, the black dots are from the MAGIC telescopes while the blue squares were measured by the *Fermi* spacecraft. The cutoff at low energies is an indication of the kinematic threshold for pion production, while the break at high energies, if this emission is from pion-decay, indicates a break in the energy spectrum of hadrons produced by the SNR blast wave (see Funk 2015).

4.8 Broad-band continuum radiation

The shock-heated plasma and relativistic CRs produce radiation that must be described if particular SNRs are to be modeled. Since the thermal X-ray line emission is coupled to the CR production through nonlinear Fermi acceleration, the broad-band continuum emission must be determined consistently with the thermal emission. The continuum processes that must be considered are synchrotron, inverse-Compton (IC), and bremsstrahlung from relativistic electrons, and pion-decay from relativistic ions interacting with the background material. Fitting the broad-band emission with a single set of parameters can strongly constraint models. This is particularly true for synchrotron because of the large lever arm between radio (from \sim GeV electrons) and X-ray synchrotron emission (from 10 – 100 TeV electrons). Care must be taken of course to ensure the observations from different instruments with different fields of view, energy resolutions, etc. are compatible.

In Fig. 8 we show a fit obtained by Ellison et al. (2012) to the broadband emission observed from SNR RX J1713.7-3946. The various emission processes are indicated and for this remnant IC emission dominates over pion-decay (p-p) at TeV energies. In other SNRs, e.g., Tycho, W44, and IC 443, pion-decay is seen to dominate. As shown by Castro et al. (2012), there are also cases, such as CTB 109, where IC and pion-decay contribute almost equally to the γ -ray emission.

First-order Fermi shock acceleration naturally puts more energy into hadrons than leptons. This is because Fermi acceleration taps the mechanical energy of the shock with near-elastic scatterings between the converging upstream and downstream flows rather than electromagnetic energy – heavy particles get more energy than light ones. All consistent models of Fermi acceleration show this. On the other hand, leptons radiate far more efficiently than hadrons. In any particular SNR, environmental factors, most importantly the density and magnetic field of the circumstellar medium, determine which of the two competing processes, IC or pion-decay, dominate.

Supernovae that explode in a dense environment, such as W44 and IC 443, are likely to show strong pion-decay emission. If the remnant is in a low density region, such as SNR RX J1713.7-3946, IC is likely to dominate. While specific features in the photon spectrum in a limited energy band (such the low-energy turnover shown in Fig. 9 for Cas A) can point to one mechanism over another, broadband fits from radio to γ -rays, which depend on both leptonic and hadronic emission, produce stronger constraints. This is particularly true when thermal X-rays are coupled to CR ion production, as in the fit shown in Fig. 8. It is important to emphasize that, in non-relativistic shocks at least, even if IC emission dominates, all consistent theories of Fermi acceleration show the underlying shock putting a large majority (e.g., 99%) of energy into hadrons.

5 Supernovae in clusters and clustered supernovae

Massive stars which are the progenitors of core-collapse SNe are typically born in dense cores of molecular clouds (e.g., Lada & Lada 2003, Krumholz 2017) and therefore are spatially and temporarily correlated. This correlation is important for global models of the interstellar medium (e.g., Heiles 1990, Cox 2005) and influences many aspects of CR physics.

Observations have revealed massive stars in both dense young compact clusters, like Westerlund 1 with a mass close to $10^5 M_{\odot}$ (e.g., Clark et al. 2008), and in unbound OB associations with stellar volume densities below $100 \text{ stars pc}^{-3}$, such as Cygnus OB2 (e.g., Wright et al. 2014).

5.1 Cosmic rays in superbubbles

Powerful stellar winds and supernovae in OB associations had been predicted to be sources of CRs (e.g., Cesarsky & Montmerle 1983, Bykov & Toptygin 1990, Bykov 2001, Lingenfelter

2017). During the early period of imaging atmospheric Cherenkov telescopes, *HEGRA* detected an excess of TeV emission with a hard spectrum spatially coincident with the Cyg OB2 region (Aharonian et al. 2002). The authors discussed the possibility that this γ -ray emission originated from TeV particles accelerated by multiple young massive stars and SNe in the Cyg OB2 region.

More recently, an extended (50 – 200 pc wide) γ -ray source was discovered with the *Fermi Large Area Telescope* in the Cygnus X region, a giant complex of molecular clouds and star-forming regions located at an estimated distance of ~ 1.4 kpc (Rygl et al. 2012). The source (dubbed the Cygnus cocoon) was identified by Ackermann et al. (2011) as a possible superbubble filled with freshly accelerated CRs. The hard emission from the Cygnus cocoon extends to 100 GeV with a flux of $(5.8 \pm 0.9) \times 10^{-8}$ ph cm $^{-2}$ s $^{-1}$ in the 1 – 100 GeV range. At a distance of 1.4 kpc, this corresponds to a γ -ray luminosity of $(9 \pm 2) \times 10^{34}$ erg s $^{-1}$. This γ -ray luminosity is below 1 percent of the kinetic power of the stellar winds in Cyg OB2, the rich OB star association located in the direction of the Cygnus cocoon.

Recently, a second extended *Fermi LAT* γ -ray source with a hard spectrum in the GeV range, possibly associated with the star forming region G25.0+0.0, was reported by Katsuta et al. (2017). The authors estimate the γ -ray luminosity of G25.0+0.0 to be about 10 times larger than that of the Cygnus cocoon for otherwise similar parameters. This implies much higher efficiencies of particle acceleration and/or radiation in the G25.0+0.0 OB association. Given the total inelastic cross section of proton-proton interaction to be about 30 mb above a few GeV, the proton cooling time would be $\sim 3 \times 10^7/n$ yr, where n is the ambient density in cm $^{-3}$. If before being released into the surrounded dense shell, GeV-TeV CRs are confined in a superbubble filled predominantly with a hot tenuous plasma, the radiative efficiency of the superbubble will be low even if the particle acceleration efficiency is high.

The age of an OB association is important for estimating the kinetic power available from SNe events. Using a population synthesis approach Martin et al. (2010) estimated the mechanical luminosity over the first 3 Myr of the life of Cyg OB2 to be $\sim 4 \times 10^{38}$ erg s $^{-1}$. Cygnus OB2 is part of the Cygnus X region and is a rich OB association with many hundreds of OB stars (e.g., Knödlseder 2000, Wright et al. 2015). Wright et al. (2014) analyzed a selected sample of *Chandra* X-ray observations of young stars and concluded that Cyg OB2 formed as a highly substructured, unbound association with a low volume density (≤ 100 stars pc $^{-3}$). They found no signs of dynamical evolution of Cyg OB2 which is inconsistent with the idea that all stars form in dense, compact clusters. On the other hand, Comerón et al. (2016) investigated the past star formation history of Cygnus OB2 using the red supergiants detectable in the near infrared as a probe to trace massive stars with initial masses between 7 and 40 M_{\odot} . They concluded that Cygnus OB2 has a history of star formation extending into the past for at least 20 Myr. This age is such that star formation started long before the latest star formation burst which produced the dense aggregate of O-type stars currently dominating the appearance of Cyg OB2.

Multiple SNe and powerful winds of early-type stars have been suggested as favorable sites of CR acceleration (see Bykov 2014, for a review). Extended superbubbles, filled with hot X-ray emitting gas, can be created by multiple clustered SNe over a time scale of $\gtrsim 10^7$ years. The bubbles will contain an ensemble of MHD shocks which may be able to strongly amplify the turbulent magnetic fields within the superbubble leading to a high efficiency (i.e., $\gtrsim 10\%$) for converting kinetic power to freshly re-accelerated CRs. This may result in a substantial temporal evolution of the CR spectra over times on the order of 10 million years. Nonlinear modeling of this process (i.e., Bykov 2001) predicted the time asymptotic CR spectrum to be a power law of index close to 2 in MeV-TeV range where the energy independent turbulent diffusion dominates the CR propagation inside the superbubble. This is consistent with the spectrum of γ -rays observed in the Cygnus cocoon if the main radiation mechanism is pion production from CR hadron interactions.

The Fermi shock acceleration mechanism assumes that CRs are confined relatively close to the shock due to a small diffusion coefficient. This strong scattering is likely provided by the turbulence produced by CR-driven instabilities, i.e., strong magnetic field amplification (e.g., Schure et al. 2012). This strong turbulence will also increase the maximum energy CRs can

obtain in the shock. Observations show that the maximum particle energies in some young isolated SNRs with shock velocities $\gtrsim 1,000 \text{ km s}^{-1}$ are typically above a TeV.

The bulk of CRs observed at Earth have GeV energies and these must escape from the SNR at late stages when the CR-generated turbulence has weakened. For core-collapse SNe, this escape is expected to occur in a superbubble. These CRs are expected to be confined and re-accelerated by multiple shocks in the superbubble (Bykov 2001, Parizot et al. 2004, Ferrand & Marcowith 2010, Bykov 2014). Recently, the *Advanced Composition Explorer CRIS* instrument discovered ^{60}Fe nuclei in CRs in the energy range 195 – 500 MeV per nucleon (Binns et al. 2016). The short ~ 2.6 Myr lifetime of ^{60}Fe suggests these nuclei originated in nearby clusters of massive stars.

It is worth noting that the observed γ -ray emission from the starburst galaxies NGC 253, NGC 1068, NGC 4945 and M82 (see Ohm 2012, 2016) show spectra with photon indexes ~ 2 . This is consistent with that observed in both the Cygnus cocoon and G25.0+0.0 but much flatter than that of the Milky Way. This may indicate that superbubble type objects are the dominant CR sources in starburst galaxies or, alternatively, that CR transport in starburst galaxies is energy independent at least up to TeV energies. Furthermore, since superbubbles are adjacent to their parent molecular complexes, the enhanced density of low-energy CRs they contain may provide ionization and heating of the dark molecular clouds. The CR energy deposition may keep the gas temperature at ~ 10 K and provide the gas ionization fraction $\sim 10^{-7}$ required by current models of the molecular chemistry in dark clouds (e.g., Grenier et al. 2015).

High-energy neutrinos produced by inelastic nuclei collisions in the Cygnus X region may have a large enough flux to be detected with the *IceCube Observatory*, as estimated by Yoast-Hull et al. (2017) using a single-zone model of CR interactions with the molecular gas. The planned observations of the Cygnus region with the high sensitivity and good angular resolution *Cherenkov Telescope Array* have the potential to provide imaging and spectra of the region between a few tens of GeV up to ~ 100 TeV (Weinstein et al. 2015). Highly informative MeV to GeV observations of the region can be performed with the planned *e-ASTROGAM* mission (De Angelis et al. 2017).

5.2 Cosmic ray acceleration by supernovae in compact clusters

Compact clusters of young massive stars are sites of SN explosions. Contrary to loose OB associations, young stellar clusters have large core star densities $\gtrsim 10^3 M_{\odot} \text{ pc}^{-3}$, with a total cluster mass $> 10^4 M_{\odot}$ within a virial radius ~ 1 pc (e.g., Portegies Zwart et al. 2010). The total mechanical power of the OB stars in such a cluster may exceed $5 \times 10^{38} \text{ erg s}^{-1}$ and will likely launch a powerful cluster wind, as modeled by Chevalier & Clegg (1985) for starburst-galaxy nuclei.

A supernova in such a cluster (see sketch in Fig. 10) may be an efficient CR accelerator. As shown by Bykov (2014) and Bykov et al. (2015), a SN blast wave, colliding with a fast wind from a compact cluster of young stars, allows the acceleration of protons to energies well above the standard limits of Fermi acceleration in an isolated SN. The proton spectrum in such a wind-SN PeVatron accelerator is hard with a large flux in the high-energy-end of the spectrum producing copious γ -rays and neutrinos in inelastic nuclear collisions. In Fig. 11 we illustrate the model predictions for the γ -ray (dashed line) and neutrino spectra (solid line) produced by a SN in a cluster similar to the galactic Westerlund 1 cluster (see Bykov et al. 2015, for details). It is estimated that the Westerlund 1 cluster may accelerate protons to $\gtrsim 40$ PeV and result in enough neutrino production to account for a few events detected by the *Ice Cube Observatory* from the inner Milky Way direction.

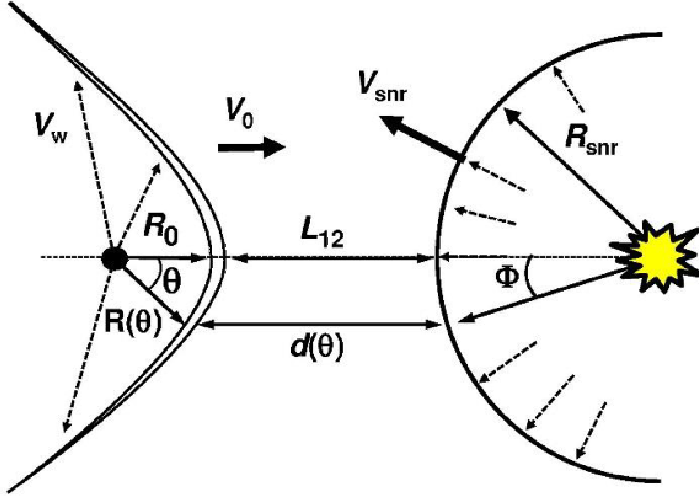


Fig. 10 A sketch illustrating the colliding shock flow geometry where the star cluster wind is impacted by a supernova shock. See Bykov et al. (2015) for details.

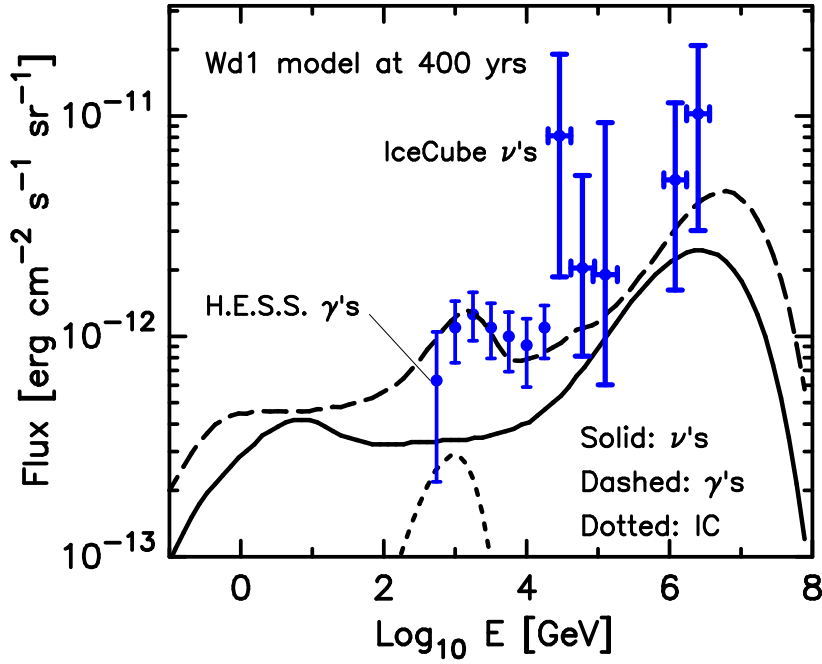


Fig. 11 Model predictions of γ -rays (dashed curve) and neutrinos (solid curve) from proton-proton interactions calculated in a colliding shock flow source of age ~ 400 yrs as given by Bykov et al. (2015). The dotted curve is the IC emission from primary and secondary electrons accelerated directly in this source. The extreme upward curvature in the neutrino spectrum above ~ 10 TeV reflects the transition from CR acceleration in the single SNR shock for low-energy particles to the more efficient acceleration for high-energy particles as they scatter back and forth between the SNR shock and the cluster wind. The data points for the H.E.S.S. source, and the five *Ice Cube* events, are presented just to illustrate the model predictions.

6 Prospects for future observational facilities

6.1 The Square Kilometer Array

The *Square Kilometer Array* (SKA, <http://skatelescope.org/>) is the next high sensitivity radio telescope scheduled for 2020 to be located in South Africa and Australia. The SKA will have an effective surface of 1 km^2 with unprecedented sensitivities of 3.36 and $0.75 \mu\text{J}/\sqrt{\text{Hz}}$ for continuum emission at two wavebands $0.05 - 0.35 \text{ GHz}$ (SKA-Low) and $0.35 - 14 \text{ GHz}$ (SKA-Mid), respectively. The SKA-Mid will have an angular resolution of 0.25 arcsecond at 1 GHz . As we have emphasized above, radio observations are essential for understanding many aspects of SN physics and the CSM and the improved sensitivity of the SKA should permit a breakthrough in SNe radio observations.

6.1.1 Radio observations of type Ia supernova explosions

As of yet, no type Ia SN explosion has been observed in the radio band. Hence, the high sensitivity of the SKA may lead to this discovery as well as the ability to follow in time the radio emission of such objects. The SKA-mid configuration should reach flux sensitivities below the upper limits obtained by the VLA for the most luminous type Ia SNe like SN 2014J or SN 2011fe.⁷ A SNIa radio detection will help to determine if the stellar system prior to the explosion is double or single degenerate. Radio emission is expected from a single degenerate case as a result of the interaction with the CSM deposited by the companion star (Wang et al. 2015).

6.1.2 Radio observations of core-collapse supernova explosions

The term core-collapse supernova (CCSN) includes a wide variety of sub-types, the names of which convey little or no information on the underlying properties of the object. For example, type IIP SNe (about half of the SNe), type IIL, I Ib, Ib/c, or IIn (see Smith 2014, for details). At present, about 50 CCSN explosions have been detected and followed in time at radio wavebands (Weiler et al. 2002, Perez-Torres et al. 2015). The SKA, with its improved sensitivity at different wavelengths and combined pointed and survey modes, is expected to detect several thousand CCSNe (Perez-Torres et al. 2015) up to a redshift $z \sim 0.25$ for the most intense type IIn SNe. With the advent of the SKA the community will be able to start statistical analysis of CCSN properties depending of their subclass type.

The SKA will also be able to monitor the closest and most intense events as it was already done with the VLA for emblematic objects like SN1987A and SN1993J. Time evolution of the radio spectrum is of particular importance to understand shock dynamics, magnetic field generation, particle acceleration in different CSM environments. These issues are intimately related to the problem of the origin of cosmic rays and make these observations particularly relevant to trigger multi-wavelength observation campaigns involving high-energy instruments like the X-ray satellites XMM-Newton or Chandra and γ -ray telescopes like the future Cherenkov Telescope Array (see next sections).

6.2 The Large Synoptic Survey Telescope

The Large Synoptic Survey Telescope (LSST) (<https://www.lsst.org/>) is a wide-field survey telescope with an 8.4-meter primary mirror currently under construction in Chile with a first light expected in 2019. It is sensitive in the $320\text{-}1050 \text{ nm}$ band and will scan the entire visible (mostly southern) sky every few nights. The LSST is an important telescope for SN optical monitoring and should obtain photosphere emission lightcurves and act as a trigger for other

⁷ The most recent anticipated instrumental performance for SKA1 is given in https://astronomers.skatelescope.org/wp-content/uploads/2017/10/SKA-TEL-SK0-0000818-01_SKA1_Science_Perform.pdf.

multi-wave length observatories. The LSST survey is designed to detect more than 100,000 core-collapse SNe, 200,000 type Ia SNe and 20,000 luminous SNe per year.

6.3 X-ray facilities

By the time the SKA comes on line, a number of telescopes very relevant for SN studies should be operating (Chandra et al. 2015). These include the Cherenkov Telescope Array (CTA) (scheduled for 2019, see Section 6.4), Chandra, NuSTAR, and hopefully Swift. XMM-Newton has a planned end date in December 2018. A planned X-ray telescope Athena+ (www.the-athena-x-ray-observatory.eu/) should be operational in 2028 when both SKA and CTA are active. There are several scientific synergies between SKA and CTA, as made clear from topics discussed in some recent joined meetings.⁸ Athena+ will be sensitive in the energy band 0.2-12 keV and will have an angular resolution of 5 arc-second at an energy < 8 keV. Sub-arcsecond angular resolution X-ray imaging combined with a sensitive high resolution spectrometry of the proposed *Lynx X-ray Observatory* (<https://www.wastro.msfc.nasa.gov/lynx/>) are very promising for the deep studies of both SNe and SNRs.

Until very recently no type Ia SN explosion has been confirmed in X-rays, but Bochenek et al. (2018) have reported the detection in Chandra data of SN 2012c, a type Ia-CSM object, i.e., a type Ia SN surrounded by very dense material. On the other hand more than 60 core-collapse SNe have been detected in X-rays (see Ross & Dwarkadas 2017, and the SNaX database at <http://kronos.uchicago.edu/snax/>).

The thermal X-ray continuum (i.e., bremsstrahlung radiation) and the thermal X-ray line emission of the shocked and heated CSM and ejecta material behind the forward and reverse shocks respectively, are tracers of the total density of the material into which the shocks are expanding as well as the shocked temperature. The evolution of the X-ray lightcurve can be used to understand the density structure of the material, and hence the mass-loss from the progenitor star (see Section 4.3 and the discussion in the referenced papers). The nonthermal radio and X-ray synchrotron emission from relativistic electrons generated by the forward and reverse shocks, can strongly constrain the shock acceleration process including the electron acceleration efficiency and the magnetic field strength in the acceleration zone. As described in Section 4.8, modeling the thermal and nonthermal radiation consistently can constrain the overall Fermi acceleration efficiency and the electron-to-proton ratio.

6.4 The Cherenkov Telescope Array

The *Cherenkov Telescope Array* (CTA, www.cta-observatory.org/) is a γ -ray observatory complex scheduled for completion in 2019. It will be located in the Canary islands and in Chile. The northern site will focus on low- and mid-energy ranges from 20 GeV to 20 TeV. The southern site will also include some large telescopes sensitive in the high-energy band up to 100 TeV. The expected γ -ray sensitivity is on the order of 0.2% Crab in 50 hours of observation at 1 TeV. At energies above 100 TeV, LHAASO (located in Tibet) is expected to reach a sensitivity of 0.01 Crab in 1 year (Di Sciascio & LHAASO Collaboration 2016).

Extending the energy range of sensitive γ -ray telescopes to 10 TeV and beyond is critical for testing CR acceleration at fast shocks. As mentioned in Section 4.8, inverse-Compton from leptons competes with pion-decay emission from hadrons at energies up to ~ 10 TeV, and which process dominates depends on often poorly constrained environmental factors. For higher electron energies however, IC emission drops due to the Klein-Nishina effect. Gamma-rays detected well above 10 TeV will almost certainly be of hadronic origin. Such a discovery would constitute a breakthrough in CR physics proving that the hadronic CR component can be accelerated quite early in the lifetime of a SNR (Schure & Bell 2013). From calculations of CR production performed in Marcowith et al. (2014) using a nonlinear Fermi acceleration model including MFA, the horizon for γ -ray detection is typically 10-20 Mpc.

⁸ See, e.g., symposium 15 at EWASS 2017, <http://eas.unige.ch/EWASS2017/>.

The detection rate of extragalactic SNe in γ -rays is uncertain since no γ -ray signal has yet been detected from such objects. Upper limits been reported (i.e., Simoni et al. 2017) and the expected number of SNe to be observed by CTA is strongly model dependent and highly uncertain. However, CTA, together with SKA, LSST and some X-ray facilities will be active at the same time. This highlights the importance of using multi-messenger radio, optical and X-ray wave bands as triggers for γ -ray monitoring for luminous sources close enough not to be absorbed by the cosmic microwave background.

7 Summary

Apart from the limited number of observed astrophysical neutrinos, and the small amount of interstellar dust so far collected, CRs are the only source of mass from beyond the solar system. Because of this, CRs convey information not obtainable from photons, and understanding their origin is of fundamental importance for astrophysics.

As we emphasize in this review, supernovae, both extragalactic, where the explosion and its aftereffect can often be witnessed, and galactic remnants, which can be studied in detail from radio to γ -rays, offer the best way to study the *in situ* acceleration of CRs. While other sources contribute to the CRs observed at Earth at some level, SNRs are clearly the source of the bulk of CRs with energies below the knee at $\sim 10^{15}$ eV (Section 1). As for the acceleration mechanism, first-order Fermi shock acceleration is the most highly developed theoretically, and has by far the most observational confirmation, of any proposed mechanism. While other mechanisms (e.g., those occurring in pulsars) may be important at some level, Fermi acceleration in collisionless shocks is most likely the prime accelerator of CRs and we concentrate on some of the current problems facing nonlinear models.

The origin of CRs with energies beyond the knee is far more uncertain than those below the knee. We discuss the possibilities of CR acceleration well beyond PeV energies by galactic sources associated with the infrequent but powerful relativistic supernovae which can accelerate CRs up to EeV (Section 3). In addition, we show how superluminous interaction powered supernovae, and normal core-collapsed SNe in clusters of young massive stars, can efficiently accelerate CRs to above PeV. At some energy above 10^{18} eV CRs are almost certainly of extragalactic origin and we mention some possible acceleration scenarios for such high energies. A critical piece of the puzzle is the transition between galactic and extragalactic CRs and understanding the production of galactic CRs in SNRs is essential for modeling this transition region.

While some aspects of CR origin and Fermi acceleration remain uncertain, we have concentrated on magnetic field amplification, Fermi acceleration in trans-relativistic shocks, acceleration in star clusters from multiple shocks, and prospects for future multi-messenger observations from radio to γ -ray energies.

Acknowledgements A.M.B, D.C.E and A.M thank the staff of ISSI for their generous hospitality and assistance. The authors thank the referees for the constructive comments. A.M. Bykov and S.M. Osipov were supported by the RSF grant 16-12-10225. Some of the modeling was performed at the “Tornado” subsystem of the St. Petersburg Polytechnic University supercomputing center. A.M. Bykov thanks R.A. Chevalier and J.C. Raymond for discussions, R.Margutti for Figure 1, and M.A. Grekov for his support with computations.

References

- Aartsen, M. G., Ackermann, M., Adams, J., et al. 2014, Physical Review Letters, 113, 101101
 Abdo, A. A., Ackermann, M., Ajello, M., et al. 2010a, Science, 327, 1103
 Abdo, A. A., Ackermann, M., Ajello, M., et al. 2010b, ApJ, 712, 459
 Abeysekara, A. U., Albert, A., Alfaro, R., et al. 2017, ArXiv e-prints
 Acero, F., Ackermann, M., Ajello, M., et al. 2016, ApJS, 224, 8
 Acero, F., Lemoine-Goumard, M., Renaud, M., et al. 2015, A&A, 580, A74
 Achterberg, A., Blandford, R. D., & Reynolds, S. P. 1994, A&A, 281, 220
 Ackermann, M., Ajello, M., Allafort, A., et al. 2013a, Science, 339, 807

-
- Ackermann, M., Ajello, M., Allafort, A., et al. 2013b, *Science*, 339, 807
- Ackermann, M., Ajello, M., Allafort, A., et al. 2011, *Science*, 334, 1103
- Aharonian, F., Akhperjanian, A., Beilicke, M., et al. 2002, *A&A*, 393, L37
- Aharonian, F., Bykov, A., Parizot, E., Ptuskin, V., & Watson, A. 2012, *Space Sci. Rev.*, 166, 97
- Aharonian, F. & Neronov, A. 2005, *ApJ*, 619, 306
- Ahn, H. S., Allison, P., Bagliesi, M. G., et al. 2010, *ApJ*, 714, L89
- Ahnen, M. L., Ansoldi, S., Antonelli, L. A., et al. 2017, *MNRAS*, 472, 2956
- Alexander, K. D., Soderberg, A. M., & Chomiuk, L. B. 2015, *ApJ*, 806, 106
- Aloisio, R., Berezhinsky, V., Blasi, P., et al. 2007, *Astroparticle Physics*, 27, 76
- Amato, E. 2014, *International Journal of Modern Physics D*, 23, 30013
- Apel, W. D., Arteaga-Velázquez, J. C., Bekk, K., et al. 2013, *Phys. Rev. D*, 87, 081101
- Archambault, S., Archer, A., Benbow, W., et al. 2017, *ApJ*, 836, 23
- Arons, J. 2003, *ApJ*, 589, 871
- Asano, K. & Mészáros, P. 2016, *Phys. Rev. D*, 94, 023005
- Axford, W. I. 1981, in *IAU Symposium*, Vol. 94, *Origin of Cosmic Rays*, ed. G. Setti, G. Spada, & A. W. Wolfendale, 339–358
- Axford, W. I., Leer, E., & Skadron, G. 1977, *Proc. 15th ICRC(Plovdiv)*, 11, 132
- Baade, W. & Zwicky, F. 1934, *Phys. Rev.*, 46, 76
- Ballet, J. 2006, *Advances in Space Research*, 37, 1902
- Bartel, N., Karimi, B., & Bietenholz, M. F. 2017, *Astronomy Reports*, 61, 299
- Bell, A. R. 1978, *MNRAS*, 182, 147
- Bell, A. R. 2004, *MNRAS*, 353, 550
- Bell, A. R. 2005, *MNRAS*, 358, 181
- Bell, A. R. & Lucek, S. G. 2001, *MNRAS*, 321, 433
- Bell, A. R., Schure, K. M., Reville, B., & Giacinti, G. 2013, *MNRAS*, 431, 415
- Berezhko, E. G. & Ellison, D. C. 1999, *ApJ*, 526, 385
- Berezhko, E. G., Elshin, V. K., & Ksenofontov, L. T. 1996, *Soviet Journal of Experimental and Theoretical Physics*, 82, 1
- Berezhnev, S. F., Besson, D., Budnev, N. M., et al. 2012, *Nuclear Instruments and Methods in Physics Research A*, 692, 98
- Berezinskii, V. S., Bulanov, S. V., Dogiel, V. A., & Ptuskin, V. S. 1990, *Astrophysics of cosmic rays*
- Bergman, D. R. & Belz, J. W. 2007, *Journal of Physics G Nuclear Physics*, 34, R359
- Bietenholz, M. F., Bartel, N., & Rupen, M. P. 2010, *ApJ*, 712, 1057
- Binns, W. R., Christian, E. R., Cummings, A. C., et al. 2014, in *APS April Meeting Abstracts*
- Binns, W. R., Israel, M. H., Christian, E. R., et al. 2016, *Science*, 352, 677
- Björnsson, C.-I. & Keshavarzi, S. T. 2017, *ApJ*, 841, 12
- Blandford, R. & Eichler, D. 1987, *Physics Reports*, 154, 1
- Blandford, R., Simeon, P., & Yuan, Y. 2014, *Nuclear Physics B Proceedings Supplements*, 256, 9
- Blandford, R. D. & Ostriker, J. P. 1978, *ApJ*, 221, L29
- Blasi, P. 2013, *Astron Astrophys Rev*, 21, 70
- Blasi, P., Epstein, R. I., & Olinto, A. V. 2000, *ApJ*, 533, L123
- Blinnikov, S. 2016a, *ArXiv e-prints* 1611.00513
- Blinnikov, S. I. 2016b, *Astronomical and Astrophysical Transactions*, 29, 129
- Bochenek, C. D., Dwarkadas, V. V., Silverman, J. M., et al. 2018, *MNRAS*, 473, 336
- Boyle, P. J., Gahbauer, F., Höppner, C., et al. 2008, *Advances in Space Research*, 42, 409
- Branch, D. & Wheeler, J. C. 2017, *Supernova Explosions*
- Brose, R., Telezhinsky, I., & Pohl, M. 2016, *A&A*, 593, A20
- Budnik, R., Katz, B., MacFadyen, A., & Waxman, E. 2008, *ApJ*, 673, 928
- Buitink, S., Corstanje, A., Falcke, H., et al. 2016, *Nature*, 531, 70
- Bykov, A. M. 2001, *Space Science Reviews*, 99, 317
- Bykov, A. M. 2014, *Astron Astrophys Rev*, 22, 77
- Bykov, A. M., Brandenburg, A., Malkov, M. A., & Osipov, S. M. 2013, *Space Sci. Rev.*, 178, 201
- Bykov, A. M., Ellison, D. C., Gladilin, P. E., & Osipov, S. M. 2015, *MNRAS*, 453, 113
- Bykov, A. M., Ellison, D. C., Gladilin, P. E., & Osipov, S. M. 2017a, *Adv. Space Res.* (2017), *ArXiv e-prints* 1706.01135
- Bykov, A. M., Ellison, D. C., & Osipov, S. M. 2017b, *Phys. Rev. E*, 95, 033207
- Bykov, A. M., Ellison, D. C., Osipov, S. M., Pavlov, G. G., & Uvarov, Y. A. 2011, *ApJ*, 735, L40
- Bykov, A. M., Ellison, D. C., Osipov, S. M., & Vladimirov, A. E. 2014, *ApJ*, 789, 137
- Bykov, A. M., Osipov, S. M., & Ellison, D. C. 2017c, *In preparation*
- Bykov, A. M. & Toptygin, I. N. 1990, *Sov. Phys. JETP*, 71
- Caprioli, D., Blasi, P., & Amato, E. 2009, *MNRAS*, 396, 2065
- Cassam-Chenaï, G., Hughes, J. P., Reynoso, E. M., Badenes, C., & Moffett, D. 2008, *ApJ*, 680, 1180
- Castro, D., Slane, P., Ellison, D. C., & Patnaude, D. J. 2012, *ApJ*, 756, 88
- Cesarsky, C. J. & Montmerle, T. 1983, *Space Sci. Rev.*, 36, 173
- Chakraborti, S. & Ray, A. 2011, *ApJ*, 729, 57
- Chakraborti, S., Ray, A., Soderberg, A. M., Loeb, A., & Chandra, P. 2011, *Nature Communications*, 2
- Chandra, P., Chevalier, R. A., Chugai, N., Fransson, C., & Soderberg, A. M. 2015, *ApJ*, 810, 32
- Chevalier, R. A. 1982, *ApJ*, 258, 790
- Chevalier, R. A. 2012, *ApJ*, 752, L2

-
- Chevalier, R. A. & Clegg, A. W. 1985, *Nature*, 317, 44
Chevalier, R. A. & Irwin, C. M. 2011, *ApJ*, 729, L6
Chugai, N. N. & Danziger, I. J. 1994, *MNRAS*, 268, 173
Clark, J. S., Muno, M. P., Negueruela, I., et al. 2008, *A&A*, 477, 147
Comerón, F., Djupvik, A. A., Schneider, N., & Pasquali, A. 2016, *A&A*, 586, A46
Cox, D. P. 2005, *ARA&A*, 43, 337
De Angelis, A., Tatischeff, V., Tavani, M., et al. 2017, *Experimental Astronomy*, 44, 25
Decourchelle, A., Ellison, D. C., & Ballet, J. 2000, *ApJ*, 543, L57
Di Sciascio, G. & LHAASO Collaboration. 2016, *Nuclear and Particle Physics Proceedings*, 279, 166
Drury, L. O. 2011, *MNRAS*, 415, 1807
Dwarkadas, V. V. 2005, *ApJ*, 630, 892
Dwarkadas, V. V. & Chevalier, R. A. 1998, *ApJ*, 497, 807
Ellison, D. C., Baring, M. G., & Jones, F. C. 1995, *ApJ*, 453, 873
Ellison, D. C. & Bykov, A. M. 2011, *ApJ*, 731, 87
Ellison, D. C., Drury, L. O., & Meyer, J. 1997, *ApJ*, 487, 197
Ellison, D. C., Moebius, E., & Paschmann, G. 1990, *ApJ*, 352, 376
Ellison, D. C., Patnaude, D. J., Slane, P., Blasi, P., & Gabici, S. 2007, *ApJ*, 661, 879
Ellison, D. C. & Ramaty, R. 1985, *ApJ*, 298, 400
Ellison, D. C., Slane, P., Patnaude, D. J., & Bykov, A. M. 2012, *ApJ*, 744, 39
Ellison, D. C., Warren, D. C., & Bykov, A. M. 2013, *ApJ*, 776, 46
Eriksen, K. A., Hughes, J. P., Badenes, C., et al. 2011, *ApJ*, 728, L28+
Falk, S. W. & Arnett, W. D. 1977, *A&AS*, 33, 515
Farber, R., Ruszkowski, M., Yang, H.-Y. K., & Zweibel, E. G. 2017, *ArXiv e-prints*, 1707.04579
Fermi, E. 1949, *Physical Review*, 75, 1169
Fermi, E. 1954, *ApJ*, 119, 1
Ferrand, G., Decourchelle, A., & Safi-Harb, S. 2012, *ApJ*, 760, 34
Ferrand, G. & Marcowith, A. 2010, *A&A*, 510, A101
Fiorito, R. B., Eichler, D., & Ellison, D. C. 1990, *ApJ*, 364, 582
Fransson, C. & Björnsson, C.-I. 1998, *ApJ*, 509, 861
Fujita, Y., Murase, K., & Kimura, S. S. 2017, *J. Cosmology Astropart. Phys.*, 4, 037
Funk, S. 2015, *Annual Review of Nuclear and Particle Science*, 65, 245
Gabici, S. & Aharonian, F. A. 2014, *MNRAS*, 445, L70
Gal-Yam, A. 2012, *Science*, 337, 927
Ginzburg, V. L. & Syrovatskii, S. I. 1964, *The Origin of Cosmic Rays*
Giuliani, A., Cardillo, M., Tavani, M., et al. 2011, *ApJ*, 742, L30
Grenier, I. A., Black, J. H., & Strong, A. W. 2015, *ARA&A*, 53, 199
Guo, Y.-Q., Tian, Z., Wang, Z., Li, H.-J., & Chen, T.-L. 2017, *ApJ*, 836, 233
Heiles, C. 1990, *ApJ*, 354, 483
Helder, E. A., Vink, J., Bykov, A. M., et al. 2012, *Space Sci. Rev.*, 173, 369
HESS Collaboration, Abramowski, A., Aharonian, F., et al. 2016, *Nature*, 531, 476
Hillas, A. M. 2005, *Journal of Physics G Nuclear Physics*, 31, 95
Horesh, A., Stockdale, C., Fox, D. B., et al. 2013, *MNRAS*, 436, 1258
Hughes, J. P., Rakowski, C. E., & Decourchelle, A. 2000, *ApJ*, 543, L61
Jones, F. C. & Ellison, D. C. 1991, *Space Science Reviews*, 58, 259
Kang, H. 2013, *Journal of Korean Astronomical Society*, 46, 49
Kang, H., Ryu, D., & Jones, T. W. 2009, *ApJ*, 695, 1273
Katsuta, J., Uchiyama, Y., & Funk, S. 2017, *ApJ*, 839, 129
Katz, B., Sapir, N., & Waxman, E. 2011, *ArXiv e-prints*
Kimani, N., Sendlinger, K., Brunthaler, A., et al. 2016, *A&A*, 593, A18
Knödseder, J. 2000, *A&A*, 360, 539
Krauss, M. I., Soderberg, A. M., Chomiuk, L., et al. 2012, *ApJ*, 750, L40
Krumholz, M. 2017, *Star Formation*
Krymskii, G. F. 1977, *Akademiia Nauk SSSR Doklady*, 234, 1306
Kulkarni, S. R., Frail, D. A., Wieringa, M. H., et al. 1998, *Nature*, 395, 663
Kundu, E., Lundqvist, P., Pérez-Torres, M. A., Herrero-Illana, R., & Alberdi, A. 2017, *ApJ*, 842, 17
Lada, C. J. & Lada, E. A. 2003, *ARA&A*, 41, 57
Lagage, P. O. & Cesarsky, C. J. 1983, *A&A*, 125, 249
Lee, S.-H., Ellison, D. C., & Nagataki, S. 2012, *ApJ*, 750, 156
Lemoine, M. 2013, in *Journal of Physics Conference Series*, Vol. 409, *Journal of Physics Conference Series*, 012007
Li, W., Leaman, J., Chornock, R., et al. 2011, *MNRAS*, 412, 1441
Lingenfelter, R. E. 2017, *Advances in Space Research*, doi:10.1016/j.asr.2017.04.006
Lipari, P. 2017, *ArXiv e-prints* 1707.02504
Lithwick, Y. & Goldreich, P. 2001, *ApJ*, 562, 279
Liu, R.-Y., Wang, X.-Y., Prosekin, A., & Chang, X.-C. 2016, *ApJ*, 833, 200
Loeb, A. & Waxman, E. 2006, *J. Cosmology Astropart. Phys.*, 5, 003
Mac Low, M.-M. & McCray, R. 1988, *ApJ*, 324, 776
Malkov, M. 2017, *ArXiv e-prints*

- Malkov, M. A., Diamond, P. H., Sagdeev, R. Z., Aharonian, F. A., & Moskalenko, I. V. 2013, *ApJ*, 768, 73
- Malkov, M. A. & Drury, L. 2001, *Reports of Progress in Physics*, 64, 429
- Marcaide, J. M., Martí-Vidal, I., Perez-Torres, M. A., et al. 2009, *A&A*, 503, 869
- Marcowith, A., Bret, A., Bykov, A., et al. 2016, *Reports on Progress in Physics*, 79, 046901
- Marcowith, A. & Casse, F. 2010, *A&A*, 515, A90
- Marcowith, A., Renaud, M., Dwarkadas, V., & Tatischeff, V. 2014, *Nuclear Physics B Proceedings Supplements*, 256, 94
- Margutti, R., Milisavljevic, D., Soderberg, A. M., et al. 2014, *ApJ*, 797, 107
- Martí-Vidal, I., Marcaide, J. M., Alberdi, A., et al. 2011, *A&A*, 526, A143
- Martin, P., Knödseder, J., Meynet, G., & Diehl, R. 2010, *A&A*, 511, A86
- Meyer, J., Drury, L. O., & Ellison, D. C. 1997, *ApJ*, 487, 182
- Meyer, J. P. & Ellison, D. C. 1999, *ArXiv Astrophysics e-prints*
- Moriya, T. J., Blinnikov, S. I., Tominaga, N., et al. 2013, *MNRAS*, 428, 1020
- Moriya, T. J. & Maeda, K. 2014, *ApJ*, 790, L16
- Morozova, V., Piro, A. L., & Valenti, S. 2017, *ApJ*, 838, 28
- Murase, K., Thompson, T. A., Lacki, B. C., & Beacom, J. F. 2011, *Phys. Rev. D*, 84, 043003
- Murase, K., Thompson, T. A., & Ofek, E. O. 2014, *MNRAS*, 440, 2528
- Nugis, T. & Lamers, H. J. G. L. M. 2000, *A&A*, 360, 227
- Ohm, S. 2012, *AIP Conf. Proc.*, 1505, 64
- Ohm, S. 2016, *Comptes Rendus Physique*, 17, 585
- Parizot, E., Marcowith, A., Ballet, J., & Gallant, Y. A. 2006, *A&A*, 453, 387
- Parizot, E., Marcowith, A., van der Swaluw, E., Bykov, A. M., & Tatischeff, V. 2004, *A&A*, 424, 747
- Patnaude, D. J., Lee, S.-H., Slane, P. O., et al. 2017, *ArXiv e-prints*
- Perez-Torres, M., Alberdi, A., Beswick, R. J., et al. 2015, *Advancing Astrophysics with the Square Kilometre Array (AASKA14)*, 60
- Petropoulou, M., Coenders, S., Vasilopoulos, G., Kamble, A., & Sironi, L. 2017, *MNRAS*, 470, 1881
- Portegies Zwart, S. F., McMillan, S. L. W., & Gieles, M. 2010, *ARA&A*, 48, 431
- Ptuskin, V. 2012, *Astroparticle Physics*, 39, 44
- Ptuskin, V. S. & Zirakashvili, V. N. 2005, *A&A*, 429, 755
- Raymond, J. C. 2017, *Space Science Reviews* (in press)
- Recchia, S., Blasi, P., & Morlino, G. 2017, *MNRAS*, 470, 865
- Reynolds, S. P. 2008, *ARA&A*, 46, 89
- Ross, M. & Dwarkadas, V. V. 2017, *AJ*, 153, 246
- Rothenflug, R., Ballet, J., Dubner, G., et al. 2004, *A&A*, 425, 121
- Rygl, K. L. J., Brunthaler, A., Sanna, A., et al. 2012, *A&A*, 539, A79
- Schure, K. M. & Bell, A. R. 2013, *MNRAS*, 435, 1174
- Schure, K. M., Bell, A. R., O’C Drury, L., & Bykov, A. M. 2012, *Space Sci. Rev.*, 173, 491
- Simoni, R., Maxted, N., Renaud, M., & Vink, J. 2017, in *IAU Symposium*, Vol. 331, *Supernova 1987A:30 years later - Cosmic Rays and Nuclei from Supernovae and their Aftermaths*, ed. A. Marcowith, M. Renaud, G. Dubner, A. Ray, & A. Bykov, 325–328
- Slane, P., Bykov, A., Ellison, D. C., Dubner, G., & Castro, D. 2015a, *Space Sci. Rev.*, 188, 187
- Slane, P., Lee, S.-H., Ellison, D. C., et al. 2015b, *ApJ*, 799, 238
- Slysh, V. I. 1992, *Astronomical and Astrophysical Transactions*, 1, 171
- Smith, N. 2014, *ARA&A*, 52, 487
- Smith, N. 2017, *Philosophical Transactions of the Royal Society of London Series A*, 375, 20160268
- Soderberg, A. M., Chakraborti, S., Pignata, G., et al. 2010, *Nature*, 463, 513
- Soderberg, A. M., Kulkarni, S. R., Berger, E., et al. 2005, *ApJ*, 621, 908
- Soderberg, A. M., Kulkarni, S. R., Nakar, E., et al. 2006, *Nature*, 442, 1014
- Sorokina, E., Blinnikov, S., Nomoto, K., Quimby, R., & Tolstov, A. 2016, *ApJ*, 829, 17
- Sveshnikova, L. G. 2003, *A&A*, 409, 799
- Tatischeff, V. 2009, *A&A*, 499, 191
- Tavani, M., Giuliani, A., Chen, A. W., et al. 2010, *ApJ*, 710, L151
- Tezhinsky, I., Dwarkadas, V. V., & Pohl, M. 2011, *ArXiv e-prints*
- Thoudam et al., S. 2016, *A&A*, 595, A33
- Uchiyama, Y., Blandford, R. D., Funk, S., Tajima, H., & Tanaka, T. 2010, *ApJ*, 723, L122
- ud-Doula, A. & Owocki, S. P. 2002, *ApJ*, 576, 413
- van Marle, A. J., Casse, F., & Marcowith, A. 2017, *ArXiv e-prints*
- Vink, J. 2012, *Astron Astrophys Rev*, 20, 49
- Vink, J. S. 2017, *ArXiv e-prints*
- Walder, R., Folini, D., & Meynet, G. 2012, *Space Sci. Rev.*, 166, 145
- Wang, L., Cui, X., Zhu, H., & Tian, W. 2015, *Advancing Astrophysics with the Square Kilometre Array (AASKA14)*, 64
- Warren, D. C., Ellison, D. C., Barkov, M. V., & Nagataki, S. 2017, *ApJ*, 835, 248
- Warren, D. C., Ellison, D. C., Bykov, A. M., & Lee, S.-H. 2015, *MNRAS*, 452, 431
- Waxman, E. 1995, *Physical Review Letters*, 75, 386
- Weiler, K. W., Panagia, N., Montes, M. J., & Sramek, R. A. 2002, *ARA&A*, 40, 387
- Weiler, K. W., Panagia, N., & Sramek, R. A. 1990, *ApJ*, 364, 611
- Weiler, K. W., Panagia, N., Stockdale, C., et al. 2011, *ApJ*, 740, 79

-
- Weiler, K. W., Sramek, R. A., Panagia, N., van der Hulst, J. M., & Salvati, M. 1986, *ApJ*, 301, 790
- Weiler, K. W., van Dyk, S. D., Discenna, J. L., Panagia, N., & Sramek, R. A. 1991, *ApJ*, 380, 161
- Weinstein, A., Aliu, E., Casanova, S., et al. 2015, *ArXiv e-prints*
- Wright, N. J., Drew, J. E., & Mohr-Smith, M. 2015, *MNRAS*, 449, 741
- Wright, N. J., Parker, R. J., Goodwin, S. P., & Drake, J. J. 2014, *MNRAS*, 438, 639
- Yadav, N., Ray, A., & Chakraborti, S. 2016, *MNRAS*, 459, 595
- Yoast-Hull, T. M., Gallagher, J. S., Halzen, F., Kheirandish, A., & Zweibel, E. G. 2017, *Phys. Rev. D*, 96, 043011
- Zimbardo, G., Amato, E., Bovet, A., et al. 2015, *Journal of Plasma Physics*, 81, 495810601
- Zirakashvili, V. N. & Ptuskin, V. S. 2016, *Astroparticle Physics*, 78, 28